Methods 148 (2018) 123–135

Contents lists available at ScienceDirect

Methods

journal homepage: www.elsevier.com/locate/ymeth

Hidden motions and motion-induced invisibility: Dynamics-based spectral editing in solid-state NMR

Irina Matlahov[a], Patrick C.A. van der Wel[a,b,*]

[a] Department of Structural Biology, University of Pittsburgh School of Medicine, 3501 Fifth Ave., Pittsburgh, PA 15213, USA
[b] Zernike Institute for Advanced Materials, University of Groningen, Nijenborgh 4, 9747 AG Groningen, The Netherlands

ARTICLE INFO

Keywords:
Solid-state NMR
Dynamics
Structural biology
Protein aggregation
Membrane proteins

ABSTRACT

Solid-state nuclear magnetic resonance (ssNMR) spectroscopy enables the structural characterization of a diverse array of biological assemblies that include amyloid fibrils, non-amyloid aggregates, membrane-associated proteins and viral capsids. Such biological samples feature functionally relevant molecular dynamics, which often affect different parts of the sample in different ways. Solid-state NMR experiments' sensitivity to dynamics represents a double-edged sword. On the one hand, it offers a chance to measure dynamics in great detail. On the other hand, certain types of motion lead to signal loss and experimental inefficiencies that at first glance interfere with the application of ssNMR to overly dynamic proteins. Dynamics-based spectral editing (DYSE) ssNMR methods leverage motion-dependent signal losses to simplify spectra and enable the study of substructures with particular motional properties.

1. Introduction

Solid state NMR (ssNMR) is widely used to study biological assemblies such as amyloids [1–10], protein complexes [11–13], membrane proteins [14–27], virus capsids [28–33], whole cells [34–36], as well as extracellular matrices, biofilms and tissues [37–39]. Several recent reviews discuss the biomolecular applications of ssNMR in more detail [40–50]. Magic-angle spinning NMR (MAS NMR) allows us to study the structure and dynamics of these biological assemblies at the atomic level, making it a powerful tool to study self-assembled biopolymers. However, challenges of biological samples that arise due to sample inhomogeneity (static disorder), dynamic disorder and increased size and complexity lead to peak overlap and crowding in the resulting NMR spectra. Multidimensional ssNMR can be used to overcome a certain degree of crowding and overlap, but has its limitations. One limitation is associated with the need for sufficiently long polarization lifetimes (i.e. slow relaxation) for the signals to survive the employed ssNMR pulse sequences. Fast relaxation not only leads to signal losses during long, multidimensional, pulse sequences, but also causes disadvantageous peak broadening in the obtained spectra. NMR relaxation is typically driven by molecular motion, which can have good and bad effects on the spectra. At the same time, fast local dynamics are responsible for the observation of narrow NMR signals for hydrated proteins above the protein glass and inharmonic dynamic transitions [51,52].

Like its liquid-state NMR cousin, the sensitivity of ssNMR to local and global motion offers unique and exciting opportunities to measure and characterize these dynamics. In solution NMR, rapid molecular tumbling in large part averages away anisotropic interactions like the dipolar coupling and chemical shift anisotropy. The suppression of these types of nuclear interactions leads to slow relaxation of the excited states, enabling the detection of spectra with narrow peaks. Site-specific variations in relaxation properties can then be attributed to differences in local dynamics. However, the molecular tumbling itself needs to be deconvoluted from internal motions of interest, which may be problematic in cases where they occur on similar time scales. Moreover, (macro)molecules with larger molecular weights experience slower tumbling, which implies stronger spin-spin interactions that shorten the relaxation times (Fig. 1C). A further extrapolation to samples lacking any molecular tumbling brings us to solid or semi-solid samples, which are the targets of ssNMR. In absence of tumbling, ssNMR relaxation measurements are used to probe *internal* rather than overall motion, spanning the nanosecond to microsecond timescales [52,53] (Fig. 1A and B). One challenge in ssNMR is the need to gain

Abbreviations: 1D, one-dimensional; 2D, two-dimensional; 3D, three-dimensional; CP, cross-polarization; CSA, chemical shift anisotropy; DARR, dipolar assisted rotational resonance; Dec, decoupling; DIPSHIFT, dipolar chemical shift correlation; DYSE, dynamics-based spectral editing; MAS NMR, magic angle spinning NMR; PDSD, proton-driven spin diffusion; PRISE, proton-relaxation-induced spectral editing; RF, radio-frequency; RINEPT, refocused insensitive nuclei enhanced by polarization transfer; ssNMR, solid state NMR; SPE, single pulse excitation; TOBSY, ThrOugh-Bond correlation SpectroscopY

* Corresponding author. Current address: Zernike Institute for Advanced Materials, University of Groningen, Nijenborgh 4, 9747 AG Groningen, The Netherlands.
E-mail addresses: p.c.a.van.der.wel@rug.nl, vanderwel@pitt.edu (P.C.A. van der Wel).

https://doi.org/10.1016/j.ymeth.2018.04.015
Received 26 February 2018; Received in revised form 5 April 2018; Accepted 16 April 2018
Available online 24 April 2018

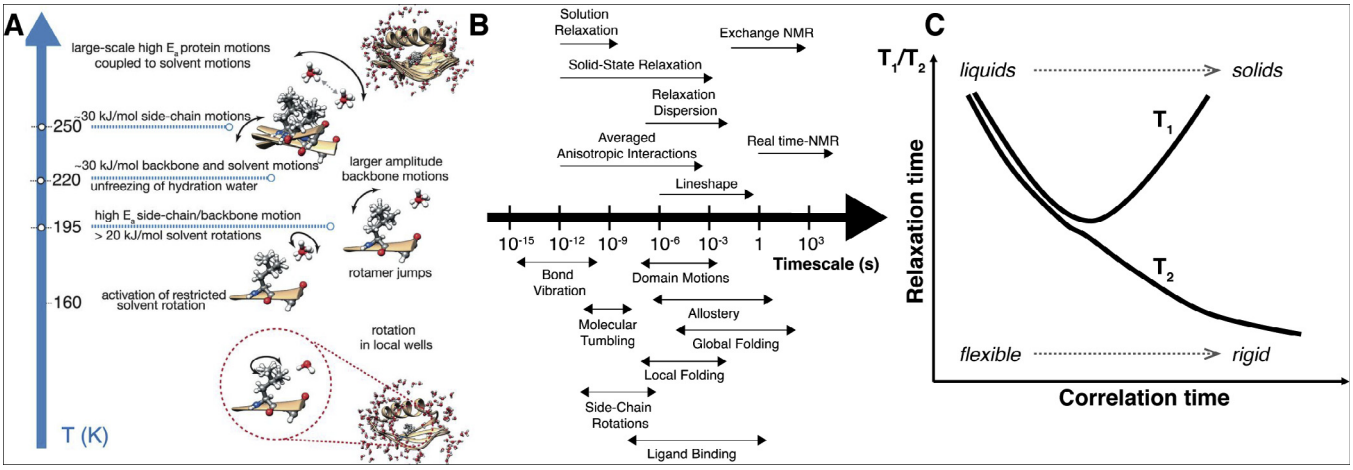

Fig. 1. Dynamics in biomolecules and their effects on ssNMR. (A) Visualization of temperature-dependent dynamics in hydrated proteins, adapted from Ref. [52]] with permission from AAAS. (B) Manifestations of different types of motion in biomolecular ssNMR. Adapted with permission from Ref. [53], Copyright 2013 American Chemical Society. (C) Schematic dependence of longitudinal (T_1) and transverse (T_2) NMR relaxation times on molecular mobility.

site-specific insights despite the presence of line-broadening anisotropic interactions. In "static" ssNMR a combination of sample alignment and heteronuclear decoupling is applied to reduce or avoid excessive line broadening (see also Section 5.2 below) [46,54–56]. In MAS ssNMR the line-narrowing effect of rapid isotropic tumbling is mimicked by the application of fast whole-sample rotation at a fixed angle (the 'magic angle') relative to the magnetic field.

SSNMR methods for performing dynamics measurements have been reviewed in detail in prior work [53,57–62]. Here, we focus on a related, but slightly different way to use and probe dynamics in biomolecular ssNMR. In particular, we discuss the approach of leveraging dynamic properties in spectral editing ssNMR experiments. Dynamics-based spectral editing (DYSE) approaches have been used to filter out, or select, the signals from parts of samples with a certain degree of dynamics or flexibility. For example, in the same sample one can separately detect the rigid cores of assemblies alongside highly flexible unfolded domains, or aggregated polypeptides alongside soluble peptides, or gel-state lipids alongside liquid-crystalline lipids. We will discuss some of the experimental approaches and the associated theoretical principles, caveats and verifications, as well as a subset of the numerous applications in the literature.

2. Effect of dynamics on ssNMR experiments

2.1. Generating the signal in ssNMR

The observed signal in 1D as well as multidimensional ssNMR spectra is determined both by the amount of polarization generated at the start of the experiment and the signal losses during the pulse sequence. NMR signals decrease over time due to relaxation processes that are sensitive to molecular motions (summarized in Fig. 1A and B). The initial signal in ssNMR experiments is generated by a preparation step ("prep" in Fig. 2A) that leverages the equilibrium polarization along the z-axis to generate observable magnetization on the xy plane for the nucleus of interest. This is accomplished by one or more radio-frequency (rf) pulses that are either followed by an acquisition period or used for additional transfers and manipulation in more complex pulse sequences (Fig. 2A and D). The simplest implementation is a single pulse excitation (SPE) experiment where we apply one 90° pulse on the nucleus of interest (e.g. ^{13}C) in order to directly measure the signal corresponding to the equilibrium polarization (Fig. 3A). This integrated signal intensity should be independent of sample mobility. However, given that experiments are almost always acquired as a series of repeated scans, the quantitative nature of the experiment is dependent on the use of sufficiently long recycle delays. Samples lacking motion have long longitudinal relaxation times, T_1 (Fig. 1C). Thus, if insufficiently long recycle delays are employed, signals from sites with slow T_1 relaxation will not be acquired at their full relative intensity.

Given the above, cross-polarization (CP; Fig. 3B) is widely used to leverage the faster relaxation and higher equilibrium polarization of protons (over ^{13}C, ^{15}N and other insensitive nuclei) to boost initial ssNMR signals [64,65]. CP relies on heteronuclear dipolar interactions to accomplish the polarization transfer. The signal transfer occurs over a "contact time" τ_{CP} during which the amount of transferred signal builds up gradually, with the build-up profile dependent on the strength of the dipolar interaction. For rigid molecules, preparative ^{1}H-^{13}C or ^{1}H-^{15}N CP has a typical contact time of hundreds of μs to several ms. However, due to the ability of dynamics to reduce the apparent dipolar coupling strengths, CP build-up profiles are heavily biased by motions. Thus, one-bound contacts that normally would yield a rapid polarization build-up (schematically illustrated in Fig. 2B as curve a) can display a much slower CP buildup when the bond is experiencing significant motion (schematically shown as curve b or c). Thus, dynamics can manifest as weaker dipolar coupling strengths than expected knowing the assignments of the coupled nuclei. CP transfers are ineffective in the presence of rapid isotropic motion, as is typical of dissolved molecules, since such dynamics average the required dipolar interactions. As we examine more below, these CP-invisible signals can often be detected with scalar-based ssNMR experiments.

In solution NMR studies, the signals of insensitive nuclei are instead enhanced by leveraging their scalar couplings to protons, typically via the Insensitive Nuclei Enhanced by Polarization Transfer (INEPT) scheme [66]. Fig. 3C shows the refocused INEPT scheme in which the first spin echo generates anti-phase state and then magnetization is transferred to the less sensitive nucleus by through-bond *J*-coupling. The second spin echo changes the transferred anti-phase state into in-phase state leading to signal enhancement. The refocusing delays τ_1 and τ_2 determine the amount of transferred signal, which is dependent on the scalar-coupling between I and S spins, J_{IS}. Thus, the choice of delays allows some control over the relative signal intensities of e.g. different types of aliphatic carbons. In the solid state, these scalar couplings are unaffected by the presence or absence of dynamics, but the relatively long spin echo periods of the INEPT scheme are highly sensitive to magnetization losses due to T_2 relaxation. In absence of homo- or heteronuclear ^{1}H decoupling (as shown in the Figure), most solid samples experience very fast T_2 relaxation unless one applies very fast MAS, (per)deuteration, or a combination thereof. As a result, conventional MAS NMR studies usually do not rely on INEPT-based signal preparation, favoring CP methods instead.

A noted feature of CP and INEPT pulse sequence blocks is that the

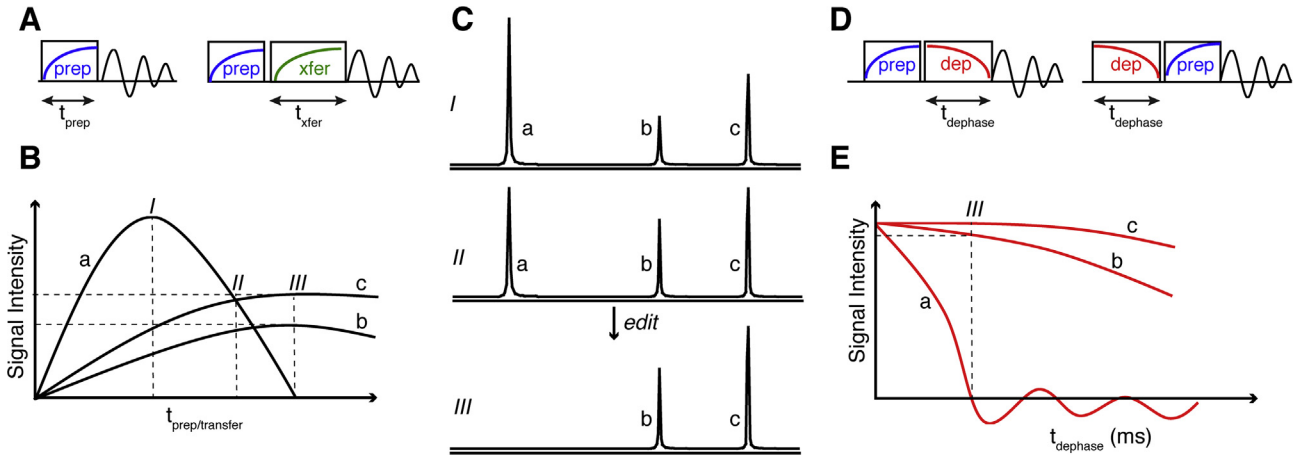

Fig. 2. Schematic representation of spectral editing approaches. (A) NMR experiments start with polarization preparation ("prep") during which magnetization is prepared on the xy plane. More complex experiments add subsequent transfer ("xfer") of this signal to other nuclei. (B) The signal intensities of different peaks (a-c) vary as a function of "prep" or "transfer" time. (C) Simulated spectrum with three peaks a-c [63], showing how changing the prep/xfer time allows one to tune the signal intensities in the spectrum (see points I, II and III in B). Note that condition III removes peak a from the spectrum. This is the concept of spectral editing. (D) Alternative spectral editing methods rely on the purposeful depolarization or dephasing ("dep") of selected signals, which can be done at different stages of the pulse sequence. (E) Signal dephasing curves as a function of dephasing time. If different nuclei dephase at different rate (as shown), spectral editing can be done by choosing a time point where signal a is zero but the others nevertheless persist (marked with III).

obtained signal varies not only with the employed contact time or delay periods, but also depends on the strengths of the dipolar and scalar couplings, respectively. Thus, different chemical groups often have different relative signal intensities, unless one purposely designs the experiment for quantitative purposes [67,68]. This is visualized schematically in Fig. 2B and C. Moreover, as explored more below, relaxation processes active during CP and INEPT schemes will affect the obtained signal intensities and make them dependent on the site-specific dynamics. In multidimensional ssNMR experiments, which rely on further polarization transfer steps ("xfer"; Fig. 2A), the final signal is also dictated by transfer efficiencies and relaxation losses during these mixing periods. Different sites with different chemical structures, geometries or dynamics will differ in their polarization transfer profiles (Fig. 2B).

2.2. Dynamics and NMR relaxation

Although they can result in NMR signal losses and line broadening, relaxation parameters do provide unique insights into the dynamics of biomolecules [53,61]. Longitudinal or spin-lattice relaxation time (Fig. 1C), T_1, indicates how long it takes the magnetization vector to reach thermal equilibrium with its surrounding [69]. Both a lack of motion or very fast motion translate into long T_1 relaxation times, with a characteristic minimum for an intermediate mobility regime (Fig. 1C). Transverse, or spin-spin, relaxation (T_2) represents the exponential decay of magnetization on the xy plane. This relaxation occurs due to mutual energy exchange between spins leading to the loss of coherence. Generally, the T_2 time increases as the mobility increases (Fig. 1C), resulting in a very short T_2 relaxation (μs scale) in rigid solids. Spin-

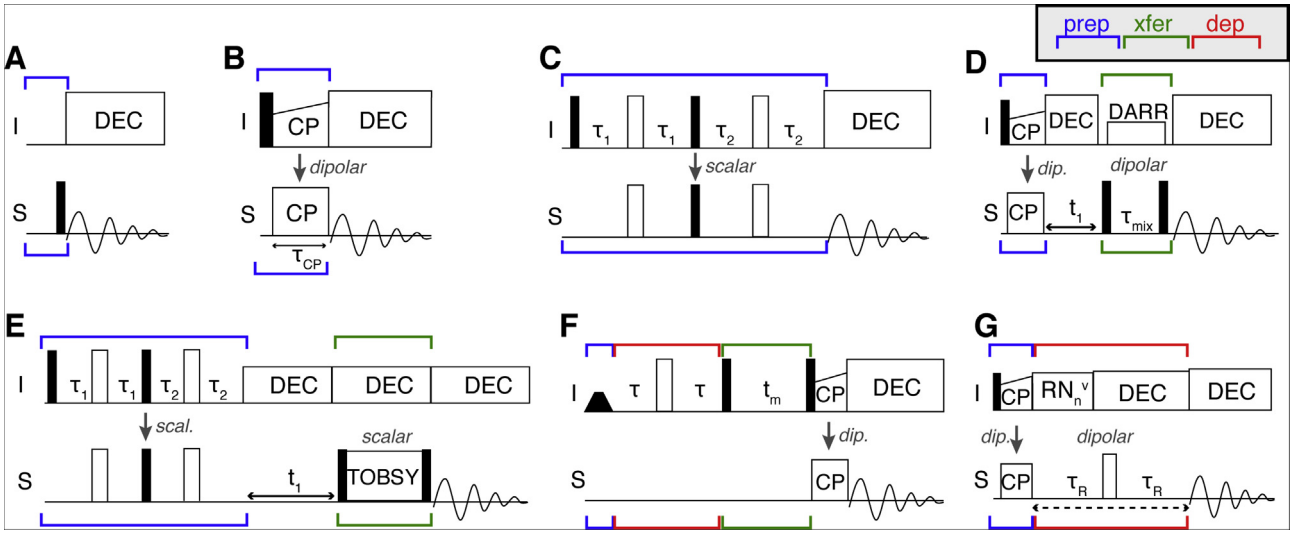

Fig. 3. Schematic pulse sequences. (A) 1D Single pulse excitation (SPE) with ^{1}H decoupling (DEC) during acquisition, which is shown as a free-induction decay (FID), (B) 1D Cross-Polarization (CP), with the CP contact time τ_{CP} indicated. (C) 1D refocused INEPT, with the τ_1 and τ_2 delay times indicated. (D) 2D CP/DARR pulse sequence for dipolar-coupling-based ^{13}C-^{13}C correlations. (E) 2D INEPT/TOBSY pulse sequence for scalar-based ^{13}C-^{13}C correlations. (F) 1D ^{1}H T_2-filtered CP-based pulse sequence used for e.g. water-filtered spectroscopy. (G) CP/DIPSHIFT experiment that correlates chemical shift and heteronuclear dipolar interaction, and can be used to measure dipolar order parameters. In all panels, filled rectangles represent 90° pulses and all empty rectangles are 180° pulses, while I and S labels represent abundant (^{1}H) and rare (^{13}C, ^{15}N) nuclei respectively. Colored brackets below/above indicate the signal preparation (blue), magnetization transfer (green) and dephasing (red) pulse sequence building blocks, as defined in the inset (top right) and Fig. 2.

lattice relaxation in the rotating frame ($T_{1\rho}$) represents the return to the equilibrium of transverse relaxation during spin-lock RF irradiation. It is most sensitive to dynamic processes occurring at frequencies close to the γB_1 RF irradiation strength, meaning that it detects slow fluctuations of 100 Hz–~3 kHz. These relaxation properties manifest themselves during distinct portions of ssNMR pulse sequences and they can thus be probed independently in specific relaxation-measuring ssNMR experiments [53,61].

2.3. Dynamics and ssNMR order parameters

Molecular motions also modulate the anisotropic interactions that govern ssNMR, including the chemical shift anisotropy (CSA), dipolar coupling as well as the quadrupolar coupling. The dynamics induce a partial averaging of the apparent anisotropy or coupling strengths, which can be measured as a motion-sensitive order parameter [28,57–59,62,70–72]. These order parameters, measured as residual CSAs, residual dipolar couplings or residual quadrupolar couplings, provide insights into both the extent and geometry of motions. In normal solution NMR studies, the rapid isotropic dynamics results in complete averaging of these couplings or anisotropies. Various ssNMR methods have been developed for measuring the CSA or quadrupolar coupling constants [73–77]. The dipolar order parameters reflect the ratio between the measured dipolar coupling strength, δ_D, and the rigid-limit dipolar coupling tensor (Eq. (1)):

$$S = \frac{\delta_D}{\delta_{D,rigid}} \quad (1)$$

The rigid limit dipolar coupling, $\delta_{D,rigid}$ depends only on the distance between two nuclei and their type. Thus, if the distance is known (e.g. for directly bonded C—H or N—H pairs) the strength of dipolar couplings provides direct insight into local molecular dynamics. One example of an approach to measure the dipolar coupling (and thus the dipolar order parameter) is represented in Fig. 3G: the dipolar chemical shift correlation (DIPSHIFT) experiment [78]. This experiment, based on a rotor-synchronized Hahn echo, was developed as a separated local field technique [79] that separates the heteronuclear dipolar coupling and chemical shift. To detect the desired heteronuclear dipolar coupling, while suppressing other undesired interactions, a variety of multiple-pulse rf pulse sequences have been employed, including several based on symmetry-based principles [71,80,81]. Experiments for measuring dipolar couplings or CSAs often involve the controlled dephasing of the site-specific NMR signals (due to the selected coupling or CSA) as schematically sketched in Fig. 2D and E. The figures illustrates schematically that the dephasing curves can vary for different peaks, for instance as a function of site-specific dynamics that modulate the effective dipolar coupling and CSA.

3. Spectral editing based on dynamics

3.1. Spectral editing

This review focuses on a class of experiments in which the above-mentioned sensitivity of ssNMR to mobility is used to filter out parts of the spectra based on their relative dynamics. This principle of purposely eliminating subsets of peaks from the spectra, based on differences in spin dynamics or other properties, is known as *spectral filtering* or *spectral editing*. Spectral editing techniques alleviate data analysis when there are many overlapping signals in the spectrum. Spectral editing can leverage different properties, such as secondary structure, mobility, chemical structure, as well as isotopic labeling patterns [82–90]. Fig. 2 schematically visualizes the concept of spectral editing, in which we aim to purposely select a subset of the signals from the top spectrum (panel C), based on their distinct properties. As seen above (panel B), the polarization buildup profile or signal transfer efficiency can vary from peak to peak (or atom to atom). Thus, one can choose a time point III (Fig. 2B) where one of the signals happens to be reduced to zero, and thus generate the edited spectrum shown in Fig. 2C (bottom). One characteristic feature, or complication, is visualized schematically in these figures: frequently some level of signal loss affects also the "desired" peaks such that spectral editing experiments can suffer from a lack of selectivity and poor signal-to-noise.

3.2. Dynamics-based spectral editing

It has long been recognized that distinct polarization preparation schemes allow for very effective spectral editing based on local motion (or lack thereof). That said, this technique is not usually described as dynamics-based spectral editing. A selection of examples is described in the following sections, but it is important to note that many other papers employ analogous methods [37,91–94]. The easiest implementation of DYSE ssNMR is simply based on the type of signal preparation that starts off the pulse sequence (Fig. 3A–C). As noted, SPE experiments (Fig. 3A) are in principle insensitive to dynamics and thereby quantitative. However, the latter depends on the allowance of sufficiently long relaxation times between scans. As such, a qualitative detection of mobility can be achieved by tuning the relaxation delay in SPE-based experiments. It is important to stress that the inter-scan equilibration of e.g. ^{13}C SPE signals does not reflect "clean" mobility-based T_1 relaxation, due to the large contributions from spin diffusion, ^{1}H couplings and other coherent processes [95–97].

As discussed above, the buildup of signal during CP (Fig. 3B) is dependent on the effective dipolar coupling and thereby can also be used to select for dynamics. An obvious implication is that CP-based ssNMR spectra of protein aggregates, amyloid fibrils or other assembled states are by definition devoid of any contribution of residual soluble molecules. This may seem obvious, but is an important characteristic of ssNMR that sets it apart from various other spectroscopic methods and may not always be self-evident to a non-expert audience.

Whilst CP experiments fail to create signal for highly dynamic or flexible molecules, the J-based INEPT experiments (Fig. 3C) accomplish the opposite. Rigid nuclei have very short T_2 relaxation times that cause their NMR signals to not survive the echo periods (at least under conventional ssNMR conditions, as discussed above). Thus, commonly, refocused INEPT (rINEPT) under MAS only yields signals for highly mobile molecules with long transverse relaxation times. As discussed in a number of recent papers, completely J-based pulse sequences can then be deployed to assign and characterize these mobile segments [98–102]. Alongside INEPT-based heteronuclear transfers, these pulse sequences often use the ThrOugh-Bond correlation SpectroscopY (TOBSY) scheme to accomplish homonuclear ^{13}C-^{13}C J-based transfers (Fig. 3E) [99,103]. The combined rINEPT-TOBSY pulse sequence is now widely used to get DYSE spectra of mobile sites in uniformly ^{13}C-labeled proteins, as a complement to e.g. 2D dipolar-based ^{13}C-^{13}C spectra. It is worth noting that certain scalar-based recoupling techniques can be combined with CP-based signals to study immobile proteins, such that it is not the case that all scalar methods *only* work for mobile segments (e.g. [104,105]).

3.3. Additional methods for DYSE pulse sequence design

The above DYSE approaches effectively take advantage of the inherent sensitivity to dynamics of these dipolar and J-based experimental methods. An alternative and complementary approach is to modify existing pulse sequences with a tailored motion-sensitivity DYSE pulse sequence element. Subsequent sections will describe examples from the literature. One obvious way to do so, is to incorporate a type of Hahn echo or inversion recovery element and to use it to selectively dephase signals with short T_2 or T_1 relaxation times. The former will select for specifically for signals with high mobility (Ref. Fig. 1C). One way such experiments have been used is to select for the ^{1}H signals of

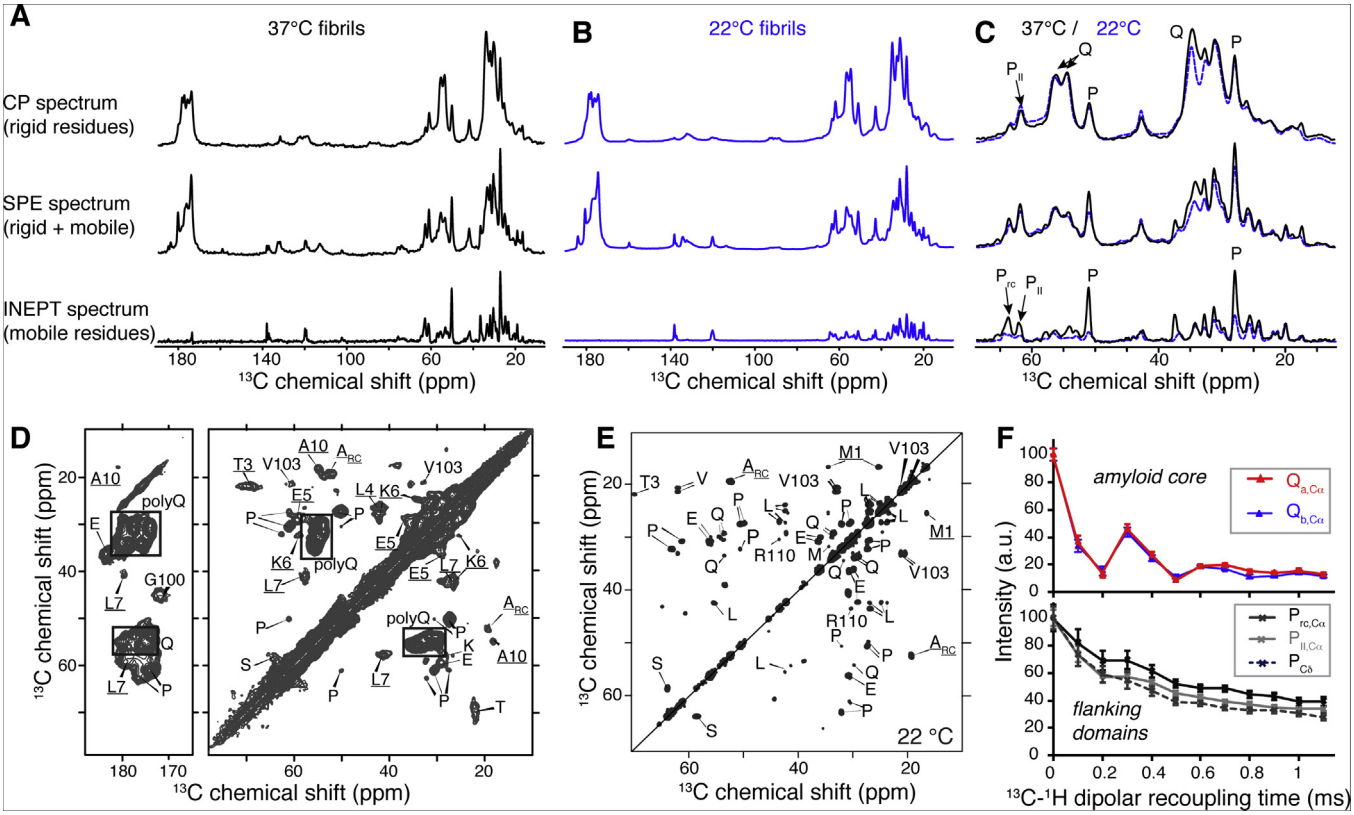

Fig. 4. 1D and 2D DYSE ^{13}C ssNMR spectra of uniformly ^{13}C,^{15}N-labeled HttEx1 fibrils. (A) Fibrils formed at 37 °C, or (B) 22 °C, are studied using CP- (rigid residues), SPE- and INEPT-based ^{13}C spectra (mobile residues). (C) Overlaid aliphatic regions, with assignments indicating the random coil (P_{rc}) and PPII-helical Pro (P_{II}). (D) 2D CP/DARR ^{13}C-^{13}C spectrum showing the amyloid core and immediately flanking immobilized segments. (E) INEPT/TOBSY 2D spectrum showing highly flexible residues in the C-terminus. (F) Differences in the ^{1}H-^{13}C DIPSHIFT dipolar dephasing curves of the rigid amyloid core and the partly immobilized flanking domains, both of which are visible in the CP/DARR 2D in (D). Adapted with permission from Ref. [7].

dynamic water molecules and liquid crystalline lipids, in water- and lipid-edited ssNMR spectra [15,86,106,107]. Longitudinal relaxation can similarly be used to selectively detect molecules with specific dynamic properties, as exemplified in the proton-relaxation-induced spectral editing (PRISE) techniques described by Tang and co-workers [84,87]. Although not directly based on dynamics, prior studies have shown how dipolar couplings and CSA parameters may be leveraged for MAS ssNMR spectral editing based on chemical structure or geometric features [83,88,89,108,109].

4. Example application to a disease-relevant protein amyloid

4.1. Huntingtin and polyglutamine expansion in human disease

In this section, we will examine our use of DYSE ssNMR experiments by discussing in some detail its usage in our work on amyloid-like fibrils formed by polyglutamine (polyQ) peptides and Huntingtin exon 1 (HttEx1) proteins. Although this section describes our workflow for these samples, this strategy has served us well across a variety of samples, ranging from membrane-associated proteins to bio-inspired nanomaterials [8,110,111]. The polyQ and HttEx1 protein aggregates exemplify the use of biomolecular MAS NMR to structurally characterize amyloid fibrils that form in various incurable neurodegenerative diseases [47,49,112,113]. Beyond the determination of their structures, ssNMR provides unique insights into the residue- or domain-specific dynamics of these types of protein assemblies, for instance in the context of Aβ amyloid fibrils [72,74]. Dynamics-sensitive ssNMR measurements have proved to be particularly essential for our understanding of HttEx1-derived fibrils and their polymorphs, in studies by ourselves and others [7,114–120]. These polyQ-containing polypeptides are of biomedical interest due to their propensity to aggregate in Huntington's disease. This autosomal disorder occurs due to expansion of a CAG repeat, which encodes a polyQ segment in the exon 1 of the gene for the huntingtin protein (Htt) [121]. The polyQ or HttEx1 polypeptides aggregate spontaneously into amyloid-like fibrils. MAS ssNMR samples are prepared by pelleting the hydrated fibrils, usually outfitted with isotopic (^{13}C,^{15}N) labeling, directly into the MAS NMR rotor, using home-built ultracentrifugal packing devices [122,123]. The resulting samples are densely packed, but retain their fully hydrated state without having been lyophilized, frozen, or otherwise dehydrated. The hydrated and unfrozen sample state is important as it retains the physiological dynamics that are leveraged in the DYSE ssNMR experiments.

4.2. MAS NMR studies

4.2.1. Qualitative 1D DYSE analysis

Basic DYSE experiments form an integral part of our initial characterization of any newly prepared sample, with the aim of qualitatively characterizing not only the structure but also mobility. Once the MAS NMR sample is at its desired experimental conditions, 1D ^{1}H SPE MAS NMR spectra are acquired. At moderate MAS rates, these ^{1}H 1D spectra do not provide much information on the protein itself, but they do permit the detection of the water signal. This is useful to qualitatively judge the hydration level and to check over time for inadvertent dehydration of the sample without need for removing and weighing the rotor. In addition, the width of the water signal can be used to ensure that the sample has not become frozen, which is an essential consideration when aiming to detect hydration-coupled dynamics [52].

Next, the signals of the ^{13}C,^{15}N-labeled protein are detected via a set

of 1D ^{13}C CP, 1D ^{13}C SPE, and 1D ^{13}C rINEPT spectra (Fig. 3A–C). Signal intensities are compared between these experiments to examine the presence of dynamic and rigid parts in the protein. Our aim is primarily to gain a qualitative understanding that allows us to decide on further experiments that probe the sample in more detail (see below). As such, the initial experiments are acquired without explicit effort to attain quantitative signal intensities, and for instance deploy standard and similar recycle delays for both CP and SPE spectra (of 2–3 s, typically).

This approach is exemplified in our comparison of different polymorphs of pathogenic HttEx1 fibrils (Fig. 4) [7]. The polymorphic fibrils differed significantly in their TEM appearance, but show little difference in the chemical shifts observed by ssNMR. Interestingly, the most notable differences prove to be in the dynamics of different domains, specifically those flanking the rigid amyloid core. These dynamic differences are easily and reproducibly observed in a comparison of 1D ^{13}C CP, SPE and rINEPT spectra (Fig. 4A–C). Before even doing time consuming quantitative analysis, 1D data clearly indicated differences in the C-terminal proline-rich domain dynamics. Previously, we observed similar dynamics in these flanking domains of shorter synthetic peptide fragments of HttEx1 [115,117]. One notable feature of the latter studies was that simple DYSE experiments helped us gain some level of insight into the domain architecture of even *unlabeled* peptide aggregates. These results are exemplified in Fig. 5, showing 1D ^{13}C CP and SPE spectra of polyQ peptides with and without Htt flanking segments [115]. This comparison showed that the polyQ core is rigid in all peptide fragments whereas the flanking domains were more mobile.

4.2.2. DYSE 2D ssNMR spectra

Further insights into the signals present in the rigid and flexible components of the 1D spectra are then obtained from 2D ^{13}C-^{13}C spectra. As a follow-up to the basic 1D CP spectrum, commonly a 2D CP-DARR [124] experiment (Fig. 3D) is performed, designed to map out one- and two-bond contacts. Samples that are judged to be quite rigid may be best probed with relatively short DARR mixing times (8–15 ms DARR mixing), but when dynamics are present it can be beneficial to employ longer mixing times (e.g. 20–25 ms mixing). The latter has often proved ideal to observe the intra-residue cross-peak patterns in both the rigid core of the HttEx1 aggregates and the more dynamic flanking regions (Fig. 4D). If there are enough signals in 1D rINEPT experiments to make it seem worthwhile, we also perform a 2D rINEPT-TOBSY experiment (Fig. 3E) to identify mobile residues. This 2D spectrum selectively detects the highly mobile C-terminal tail of HttEx1 (Fig. 4E). The 2D spectra alone already can provide residue-type assignments to the 1D spectra and their dynamic information. For the assignments of amino acid type and secondary structure we have found the PLUQ program useful [125]. For multidomain proteins such as HttEx1, distinct domains commonly have distinct amino acid compositions. As such, the identification of the relative mobilities of specific amino acid types can often already reveal (or at least suggest) the secondary structure content and motional characteristics of individual domains. For many biological systems, this type of information is highly important, yet can be very difficult to detect by other spectroscopic methods.

4.2.3. Relaxation-filtered ssNMR to probe solvent accessibility

The domain-specific and residue-specific dynamics are often attributable to the degree of solvent exposure of different parts of the protein. As discussed above, one type of DYSE spectra have been used to probe this very feature. T_2-filtered ^{13}C MAS ssNMR can suppress rigid protons and probe water accessibility (Fig. 6A and B), via a basic pulse sequence as shown in Fig. 3F [107]. A Hahn-echo removes all proton

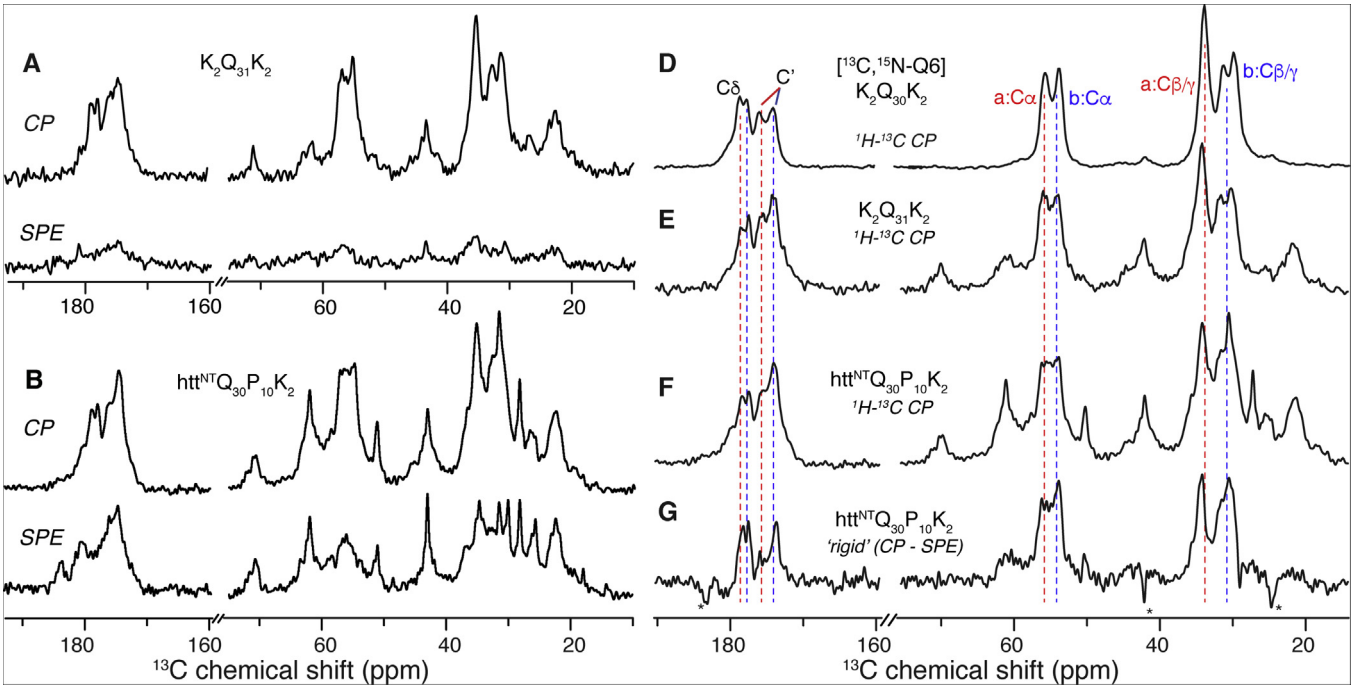

Fig. 5. 1D DYSE ^{13}C spectra on polyQ amyloid fibrils with and without Htt flanking domains. (A) ^{1}H-^{13}C CP (top) and ^{13}C SPE (bottom) of unlabeled $K_2Q_{31}K_2$ fibrils. The CP signal of this rigid sample is much enhanced relative to the SPE spectrum with a 3 s recycle delay. (B) Analogous spectra for unlabeled $htt^{NT}Q_{30}P_{10}K_2$ fibrils outfitted with htt^{NT} and oligoproline flanking segments. The SPE spectrum is now much enhanced and dominated by the flanking segments due to their increased mobility. (D–G) Comparison of CP-detected "rigid signals": (D) singly ^{13}C,^{15}N-labeled Gln6 in $K_2Q_{30}K_2$, (E) unlabeled $K_2Q_{31}K_2$ fibrils (from A), (F) $htt^{NT}Q_{30}P_{10}K_2$ CP spectrum (from B). (G) Subtraction of the $htt^{NT}Q_{30}P_{10}K_2$ SPE spectrum from (F) reveals the most rigid sites in this sample (positive signals). The most mobile signals yield negative peaks. Note that the "rigid" peaks match the pattern of labeled or unlabeled polyQ in (D and E). Thus, DYSE filtering allows the dissection of overlapping dynamic and rigid parts of samples, even in absence of labeling. Adapted with permission from Ref. [115] Copyright 2011 American Chemical Society.

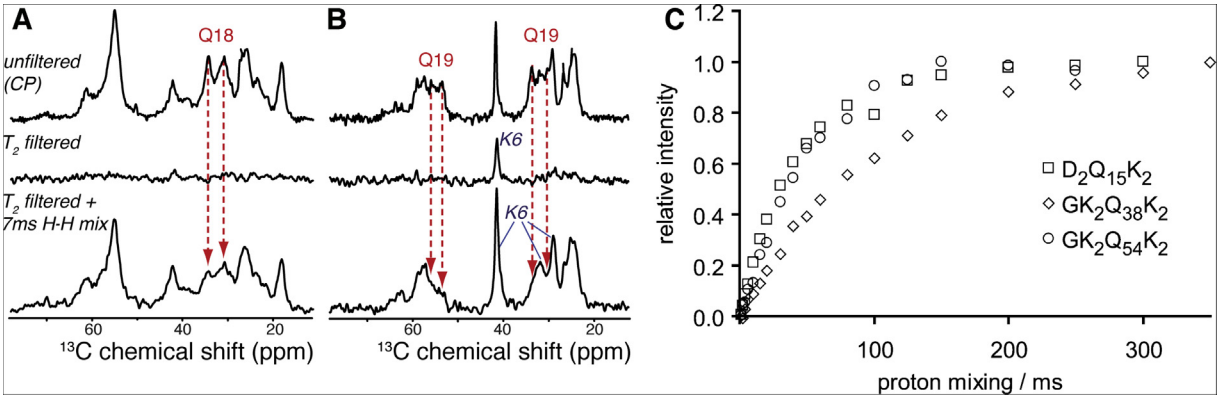

Fig. 6. Water-edited NMR spectra on polyQ-related amyloids. (A and B) ^{1}H-^{13}C 1D CP spectrum of residue-specifically labeled Htt^{NT}Q$_{30}$P$_{10}$K$_2$ peptide fibrils with different residues in Htt^{NT} and the polyQ domain ^{13}C,^{15}N-labeled. A 3 ms ^{1}H T$_2$ filter eliminates virtually all signals (middle). 7 ms ^{1}H-^{1}H mixing (bottom) allows ^{1}H polarization transfer from mobile water into the peptide fibrils, in which the Gln signals are suppressed relative to the labeled sites in the flanking domain Htt^{NT}. Panels (A and B) are adapted with permission from Ref. [115] Copyright 2011 American Chemical Society. (C) Buildup of water-edited intensity in the aliphatic spectral region for three polyQ aggregates, which was used to probe solvent access and approximate particle sizes. Adapted from Ref. [114] with permission from Elsevier.

signals from the rigid parts of the sample, leaving only mobile protons from the solvent (Fig. 6B). A longitudinal ^{1}H-^{1}H spin diffusion period before cross-polarization allows magnetization transfer from mobile water molecules to the fibrils. Consistent with the observed difference in C-terminal domain dynamics, water-edited ssNMR experiments indicated that the C-terminal domains of HttEx1 polymorphs vary in their exposure to solvent [7]. Another study of polyQ peptides with different Gln lengths [114] used similar methods (Fig. 6C) to observe that the polyQ fibril core was dehydrated and had a width is 7–10 nm.

4.2.4. Beyond the DYSE analysis

Above we stressed the fact that most of these DYSE experiments should be considered qualitatively indicative of dynamics and cannot replace a more comprehensive and quantitative analysis. As such it is advisable to use the DYSE spectra as a precursor to more detailed experiments. For instance, to verify qualitative analyses of dynamics obtained via DYSE, we performed targeted quantitative measurements of dynamics. This included ^{15}N T$_1$ measurements on the backbone and side chains, DIPSHIFT-based ^{15}N-^{1}H dipolar coupling measurements, as well as DIPSHIFT-based ^{13}C-^{1}H dipolar coupling measurements (Fig. 4F) [7,117,119]. These measurements supported and confirmed the attribution of rigidity and dynamics that were qualitatively deduced from the qualitative DYSE spectra. The determination of order parameters (i.e., the presence or absence of dynamic averaging of dipolar couplings) is also important for subsequent structural measurements, as dynamic averaging modulates the expected polarization build-up profiles typical of distance measurements. This was observed, for instance, in our recent analysis of the PDSD-based magnetization transfer behavior in the polyQ and flanking domains of HttEx1 [7].

4.3. Biological implications

The abovementioned dynamics information does not provide as comprehensive, quantitative or detailed a picture as has been obtained for a number of other proteins [24,52,58,126,127]. Nonetheless, the obtained results provided a unique perspective on these polyQ expansion disease-related protein deposits [7,115–120]. First of all, the ssNMR spectra reveal a dramatic range of dynamics across the length of the HttEx1 polypeptide. The polyQ domain is highly rigid, while its immediate flanking regions experience increased motion yet are still immobilized. In the C-terminal segment, this mobility gradually increases up to an essentially disordered C-terminal tail. Combined with various structural measurements, these dynamics proved invaluable to efforts to develop a structural model of the aggregates (Fig. 7). It is worth noting that the static and dynamic disorder of HttEx1 in both its native and fibrillar state has thus far limited the ability of advanced cryoEM methods to delineate its structure in any detail [128–130]. Changes in dynamics that were apparent from the DYSE spectra (Fig. 4) pointed us to a type of *supramolecular* polymorphism [131] being behind the HttEx1 fibril polymorphs.

5. Other applications and examples

In Section 5 we discuss a selection of other applications of DYSE-type spectra from the literature. We note again that there are numerous examples not examined here, due to space considerations rather than lack of importance. Many studies that employ these methods do not explicitly describe them as dynamics-based spectral editing. That said, Fig. 8 is reproduced from a report that does explicitly discuss the development of a DYSE pulse sequence for selecting the signals of dynamic residues in 2D and 3D ssNMR spectra [89]. The pulse sequence (Fig. 8A) illustrates some notable design features to achieve the optimized reproduction of mobile residues' peaks in the DYSE spectrum. The initial "preparation" of the ^{13}C signals is optimized for detection of more mobile signals by preceding the CP contact time with a ^{13}C 90° pulse, effectively combining CP with SPE. Moreover, a subsequent ^{13}C-^{13}C mixing period is added to distribute signal from highly polarized rigid carbons to more dynamic sites. Next, the DYSE is based on a rotor-synchronized Hahn echo with an asymmetric gated ^{1}H decoupling period. This pulse sequence construct selects for methyl groups and CH$_2$ and CH carbons featuring enhanced dynamics, while suppressing other, more rigid, protonated carbons. Fig. 8B shows the application of this approach in a 2D ^{13}C-^{13}C spectrum of the crystalline model protein GB1, but this pulse sequence element could similarly be included in other 2D and 3D ssNMR experiments.

5.1. MAS NMR studies of integral and peripheral membrane proteins

One pivotal paper demonstrated the power of combining dynamics-selective CP- and INEPT-based MAS NMR spectroscopy on the 52-residue phospholamban, studied in lipid bilayers [99]. Baldus and coworkers show how one can separately observe the unfolded extramembrane domain and the folded membrane-bound domains of the protein, using scalar (i.e. INEPT-based) and dipolar (i.e. CP-based) 1D (Fig. 9A and B) and 2D spectra (not shown; see [99]). Moreover, a suite of scalar-based pulse sequences is described, for the purposes of performing site-specific assignments in multidimensional spectra.

We have applied a subset of such methods to a peripherally bound

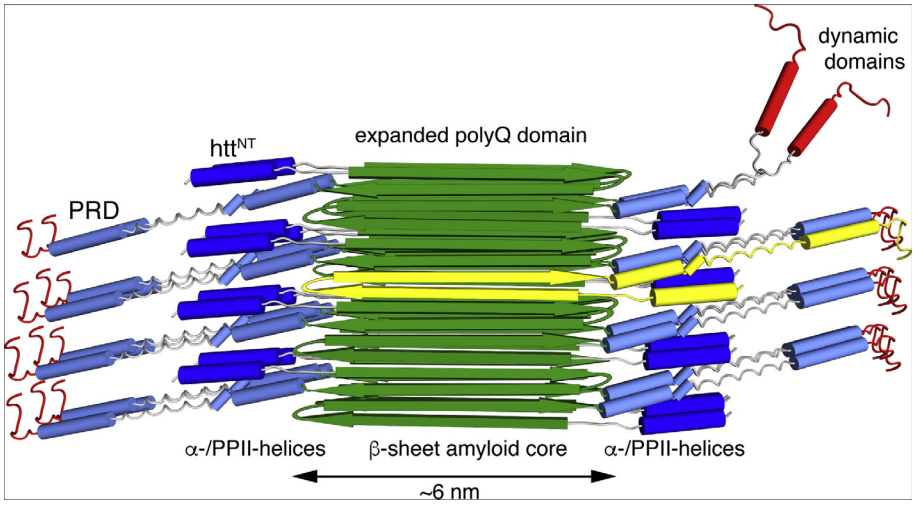

Fig. 7. Model structure of HttEx1 fibrils informed by a combination of structural and dynamic ssNMR experiments, including the DYSE data discussed above. Adapted with permission from Ref. [7].

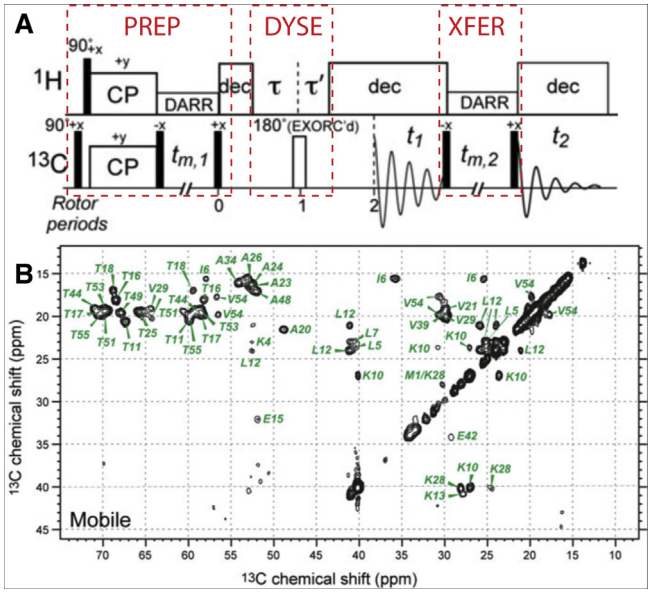

Fig. 8. 2D DYSE ssNMR on U-^{13}C,^{15}N-labeled protein crystals. (A) Spectral editing pulse sequence for selecting methyl groups and dynamic protonated residues. The polarization preparation (PREP) is optimized for generating signals from mobile sites (see text), while the dynamic filtering (DYSE) is based on ^{1}H-^{13}C dipolar couplings. ^{13}C-^{13}C polarization transfer (XFER) is effected by DARR or PDSD transfers. (B) Application of the above pulse sequence on a 2D ^{13}C-^{13}C spectrum of crystalline GB1 at 10 kHz MAS and 600 MHz (^{1}H). Adapted with permission from Ref. [89].

membrane protein [22]. In particular, our studies examined the structure and dynamics of mitochondrial cytochrome *c* bound to vesicles containing the negatively charged lipid cardiolipin. One notable observation was that the uniformly ^{13}C,^{15}N-labeled lipid-bound protein was close to invisible in both CP- and INEPT-based ^{13}C 1D spectra (Fig. 9C–E). Those spectra were dominated by signals from the unlabeled phospholipids, which were in a liquid-crystalline bilayer state. The implication was that the membrane-bound protein is sufficiently dynamic that conventional CP experiments are ineffective, likely due to a combination of fast relaxation and reduced dipolar order parameters. At the same time, it lacked the high mobility associated with the slow T_2 relaxation necessary for the non-^{1}H-decoupled INEPT scheme to yield signal. Thus, the protein occupied an intermediate motional regime where its ssNMR (^{13}C) signals could only be efficiently observed by direct ^{13}C SPE (Fig. 9C). These observations point to a crucial point when it comes to the deployment of the CP- and INEPT-based spectral editing approaches: there is a "grey zone" of intermediate time scale dynamics that may be missed by both those methods. In the case at hand, we interpreted the dynamic properties of the peripheral protein to suggest that it was not fully unfolded in the membrane. This conclusion was supported by FTIR and lower-temperature 2D and 3D MAS NMR studies (e.g. the grey spectrum in Fig. 9D and Ref. [22]).

INEPT-based spectroscopy requires a very high degree of flexibility, which typically is associated with a lack of secondary structure. However, CP- based ssNMR also offers chances to distinguish different levels of dynamics, as explored and illustrated in a number of different studies [132–135]. Huster and co-workers [133] showed in MAS as well as static ssNMR of a membrane-embedded GPCR how the observed peaks and line-shapes varied as a function of the employed CP contact time. Consistent with these changes reflecting mobility differences, the CP signal build-up was shown to correlate to dipolar order parameters, measured using DIPSHIFT experiments.

The dynamic properties of membrane proteins enable the application of ^{1}H-detected MAS NMR approaches at moderate MAS rates that would not be feasible on rigid proteins. This was explored in recent papers [136,137], examining both integral membrane proteins as well as peripherally bound myelin basic protein (MBP). 2D and 3D ^{1}H detected experiments were shown to be effective for selectively studying the most flexible protein segments, without need for deuteration. It is worth noting that also the liquid crystalline lipid bilayer itself is characterized by high dynamics that enable high-quality 1D and multidimensional ^{1}H-detected experiments as well as INEPT-based spectroscopy [138–140].

Membrane protein studies have also seen common applications of DYSE based on ^{1}H T_2 relaxation properties [15,107,141]. In context of fluid membrane samples not only the solvent molecules are highly mobile, but also the liquid crystalline lipid acyl chains. As such, both can be retained in the T_2-filtered experiments, enabling detection of both solvent-protein and lipid-protein interactions [86,142]. Note that the latter does imply that multidimensional spectroscopy may be required for dissecting the origins of the transferred ^{1}H signals (which may not be needed in samples where only water ^{1}H signal is retained).

5.2. Dynamics-based spectral editing in oriented membrane ssNMR

Although most of this review focuses on MAS NMR studies, similar methods apply in the area of oriented-membrane static ssNMR [133,134]. One example is a ssNMR study of N-terminal FMN binding

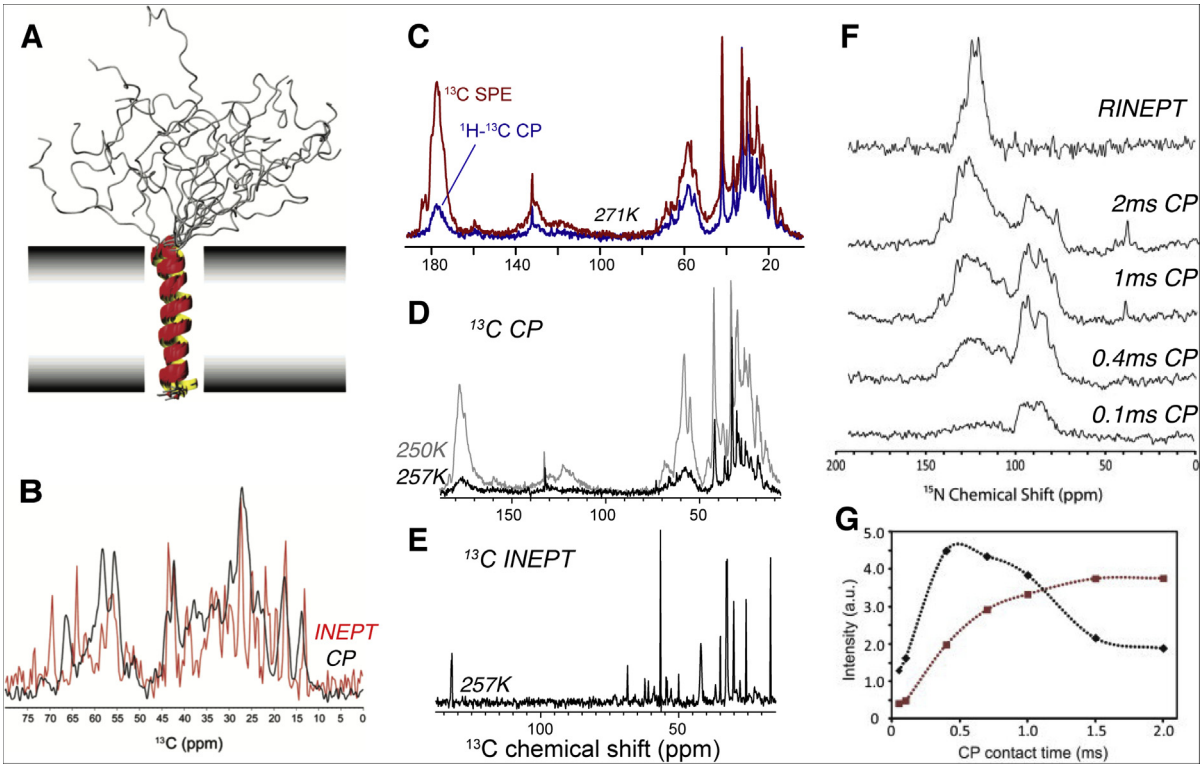

Fig. 9. Examples of DYSE ssNMR on membrane-associated proteins. (A) Model of monomeric mutant phospholamban (AFA-PLN) with an α-helical transmembrane domain and a dynamic unfolded extra-membrane segment. (B) 1D ^{1}H-^{13}C CP (black) and INEPT (red) spectra of AFA-PLN in DMPC bilayers at 11 kHz MAS and 30 °C. A and B were adapted with permission from Ref. [99] Copyright 2005 American Chemical Society. (C) ^{13}C SPE and CP MAS NMR spectra of reduced U-^{13}C,^{15}N-cytochrome *c* associated with cardiolipin-containing lipid vesicles, at 271 K. (D) 1D ^{13}C CP spectra of lipid-bound cytochrome *c* at 250 K (grey) and 257 K (black). (E) ^{13}C INEPT spectrum of the same sample, at 257 K. In the unfrozen sample, protein peaks are absent or weak in both CP and INEPT spectra. Panels C–E adapted from Ref. [22], with permission from Elsevier. (F) Oriented ^{15}N CP NMR spectra of a membrane-bound fragment of NADPH-cytochrome P450 oxidoreductase in magnetically aligned bicelles obtained via rINEPT or CP with variable contact times. (G) CP contact-time dependency of the relative intensities of the intra- and extra-membrane domains of the protein. Adapted from Ref. [134], with permission from Elsevier.

domain of NADPH-cytochrome P450 oxidoreductase in a native membrane-like environment [134]. This N-terminal fragment features a transmembrane domain and an extracellular domain, both of which are α-helical in structure. Embedded in magnetically aligned bicelles, the two domains are distinct in their ^{15}N chemical shifts due to the different orientations of the respective α-helices. Importantly, for the current review, the dynamic differences between the domains allowed their NMR signals to be selectively observed. As shown in Fig. 9F, ^{1}H-^{15}N INEPT generates only signal from highly dynamic residues outside the membrane. Further dynamic selectivity was achieved by varying the CP contact time. Short contact times effectively generate ^{15}N signal for the least dynamic transmembrane α-helix, whilst longer contact times are necessary to polarize the dynamic extra-membrane domain (Fig. 9F and G). The differential build-up profiles of the domains enable spectral editing by dynamics. Analysis of the buildup curves (Fig. 9G) suggested that the transmembrane helix experiences rotational diffusion of the whole helix and fluctuation of the helical director axis.

5.3. MAS NMR studies of disease-related protein aggregates

In Section 4 we examined in detail the application of DYSE methods in polyQ-expanded protein aggregates. Here we show a few examples of similar methods applied to other polypeptide or protein aggregates, from among many more in the ssNMR literature. The structure of aggregated FUS protein implicated in ALS and FTD neurodegeneration was recently studied by ssNMR [9]. Like the abovementioned polyQ-based aggregates, this protein was found to feature a well-defined rigid core decorated with dynamic non-amyloid flanking regions. The former was detected and characterized using CP-based spectroscopy (Fig. 10A and B), which yielded the 3D structure shown in Fig. 10D. INEPT-based spectroscopy revealed the signals from the dynamic flanking regions (Fig. 10C). Similar features have been reported for several other amyloid proteins featuring flexible and dynamic flanking regions [100,101,143,144]. For instance, MAS NMR studies of human and fungal prion proteins [100,132,145], combining CP- and INEPT-based methods, showed that only a defined portion of the polypeptide chain ended up in the rigid amyloid core (Fig. 10E). As also discussed in context of membrane protein studies, the flexible regions not only enable 2D and 3D J-based spectra to be acquired, but also facilitate selective detection via ^{1}H-detected MAS NMR at moderate MAS rates and without extensive deuteration [101,143].

Even simple 1D SPE-based spectra can permit the detection of extensive flexibility as a proxy for solvent accessibility. Fig. 10F shows an example in ssNMR studies of amyloid-like fibrils formed by a short fragment of the yeast prion protein Sup35. In the fibrils, the peptides co-assemble in three distinct conformations with each their distinct ssNMR chemical shifts. While probing these fibrils with simple 1D ^{13}C spectra, employing both CP- and SPE, it became apparent that one residue in one of the three peptide conformers yielded surprisingly high (and narrow) peaks in ^{13}C direct excitation spectra. The behavior of this amino acid was strikingly different from the rest of the fibrillar peptides, and also from “amyloid-like” crystals of the same peptide. The difference is especially appreciated when using relatively short recycle delays that effectively filter out sites with slow ^{13}C T_1 relaxation, a feature typical of immobile carbon atoms. One caveat in this type of analysis (at moderate MAS rates) is that the T_1 relaxation of rigid carbons can be enhanced by proximity to “relaxation sinks” such as mobile methyl groups [95–97]. In such cases, complementary dynamics

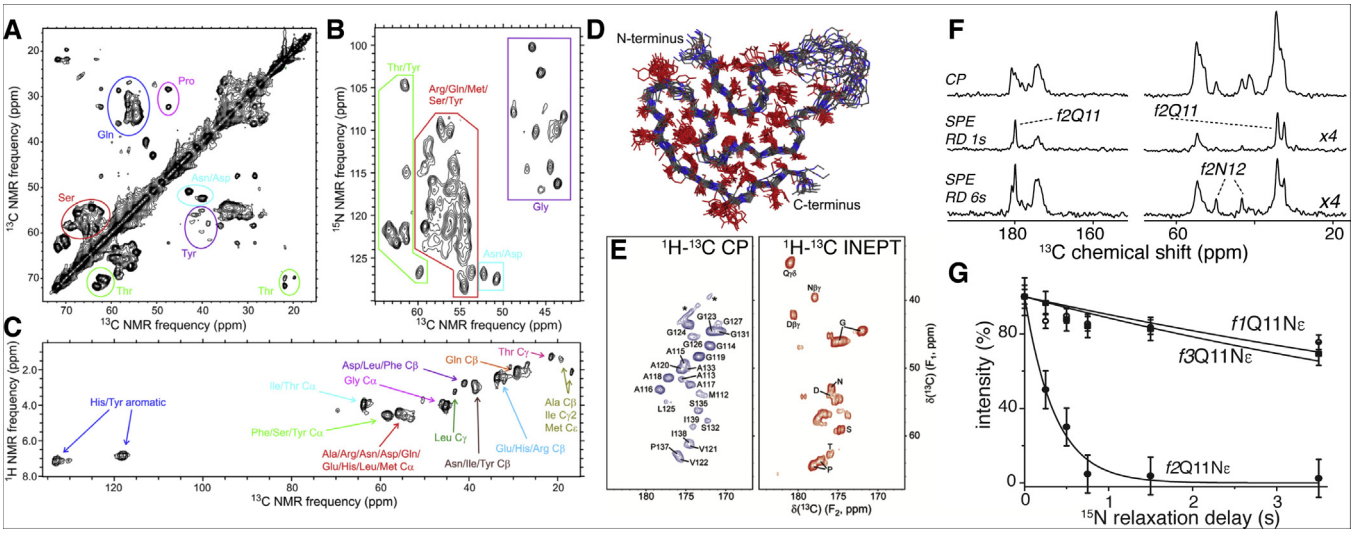

Fig. 10. DYSE ssNMR on amyloid fibrils. (A and B) CP-based 2D spectra of the immobilized core of aggregated FUS. (C) INEPT-based HETCOR spectrum of FUS aggregates, featuring only signals from flexible residues. (D) SSNMR-based structure of the immobilized FUS amyloid core. Adapted from Ref. [9] with permission from Elsevier. (E) CP- and INEPT-based spectra of the rigid and flexible regions of prion protein aggregates. Adapted with permission from Ref. [132] Copyright 2010 American Chemical Society. (F) 1D CP and SPE (scaled x 4) spectra with recycle delays as indicated for GNNQQNY amyloid fibrils. (G) ^{15}N T_1 relaxation of GNNQQNY Gln side chain nitrogens, supporting the apparent mobility of conformer-2 Gln-11 identified in the 1D spectra in (F). Adapted with permission from Ref. [146] Copyright 2011 American Chemical Society.

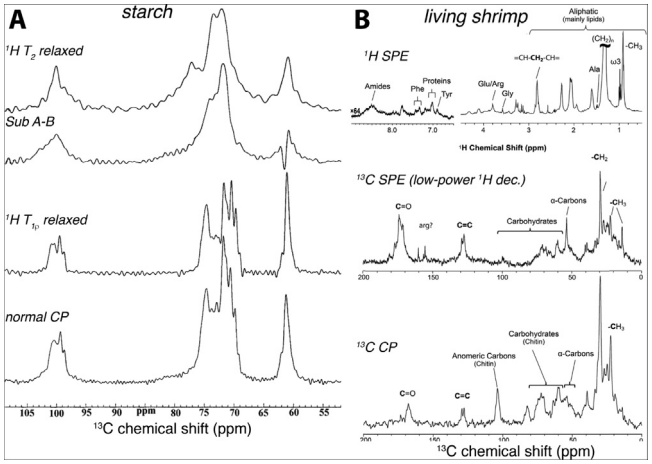

Fig. 11. DYSE ssNMR on other biological systems. (A) 1D PRISE spectra of starch, comparing normal CP with ^{1}H relaxation filtered CP variants. Adapted with permission from Ref. [87] Copyright 2003 American Chemical Society. (B) 1D NMR spectra of living *H. azteca* shrimp obtained using ^{1}H SPE NMR (top), ^{13}C SPE with low power decoupling (to suppress true solids), and ^{13}C CP (bottom) to reveal solid components. Adapted from Ref. [147] – Published by The Royal Society of Chemistry.

measurements can be applied, such as ^{15}N T_1 measurements that were performed here (Fig. 10G).

5.4. Dynamic editing in ssNMR studies of other biological assemblies

The above sections have focused on the application of DYSE experiments to proteins or peptides. However, these techniques have proved equally effective in non-polypeptide-based biological samples. A few examples are discussed in this section. In 2000, Tang and coworkers coined the term proton relaxation-induced spectral editing (PRISE) for a set of ^{1}H relaxation-sensitive MAS NMR techniques to dissect the dynamics of plant cell walls and other biological materials [84,87,148]. Fig. 11A shows a subsequent application to polysaccharides in native starch granules [87]. Another area where DYSE-type applications prove valuable is in the study of whole cells and even organisms. One example is shown in Fig. 11B, based on the study of the fresh water shrimp *Hyalella azteca* using comprehensive multiphase (CMP) NMR enabled by a specifically designed MAS probe [147,149]. Many other applications have been reported, including studies of the mobile components of lipids and other biomolecules in various conditions, such as whole-cells, biomaterials, organic matter, as well as *in vitro* [36,82,84,138–140,147,149–151].

6. Conclusion

In this review, we discussed a diverse group of ssNMR experiments that can be considered as Dynamics-based Spectral Editing (DYSE) experiments. The DYSE approach is used to selectively detect sites with a certain degree of flexibility. We have seen that 1D and 2D DYSE experiments lead to a qualitative understanding of distinct motions in different parts of the biological samples. Although qualitative in nature, the DYSE approach provides valuable new insights inaccessible by other spectroscopic or structural techniques. It also facilitates the informed selection of further quantitative and more time-consuming dynamics studies. Our examples showed that by applying filtering techniques it is possible not only to detect rigid or mobile domains in multidomain proteins but also their accessibility to solvent and lipids. These spectral editing techniques are implemented in various complex systems such as integral or peripheral membrane proteins, amyloids, biominerals, and protein complexes.

Acknowledgements

This work was supported by the National Institutes of Health R01 AG019322, R01 GM112678, R01 GM113908, and S10 grant OD012213-01. The authors acknowledge fruitful discussions with past and current members of the Van der Wel research group.

References

[1] A.T. Petkova, R.D. Leapman, Z. Guo, W.-M. Yau, M.P. Mattson, R. Tycko, Self-propagating, molecular-level polymorphism in Alzheimer's beta-amyloid fibrils, Science (New York, NY) 307 (2005) 262–265, http://dx.doi.org/10.1126/science.1105850.

[2] C.P. Jaroniec, C.E. MacPhee, V.S. Bajaj, M.T. McMahon, C.M. Dobson, R.G. Griffin, High-resolution molecular structure of a peptide in an amyloid fibril determined

by magic angle spinning NMR spectroscopy, Proc. Natl. Acad. Sci. U.S.A. 101 (2004) 711–716, http://dx.doi.org/10.1073/pnas.0304849101.
[3] A.W.P. Fitzpatrick, G.T. Debelouchina, M.J. Bayro, D.K. Clare, M.A. Caporini, V.S. Bajaj, et al., Atomic structure and hierarchical assembly of a cross-β amyloid fibril, Proc. Natl. Acad. Sci. U.S.A. 110 (2013) 5468–5473, http://dx.doi.org/10.1073/pnas.1219476110.
[4] M.A. Wälti, F. Ravotti, H. Arai, C.G. Glabe, J.S. Wall, A. Böckmann, et al., Atomic-resolution structure of a disease-relevant Aβ(1–42) amyloid fibril, Proc. Natl. Acad. Sci. U.S.A. 113 (2016) E4976–84, http://dx.doi.org/10.1073/pnas.1600749113.
[5] M.D. Tuttle, G. Comellas, A.J. Nieuwkoop, D.J. Covell, D.A. Berthold, K.D. Kloepper, et al., Solid-state NMR structure of a pathogenic fibril of full-length human α-synuclein, Nat. Struct. Mol. Biol. 23 (2016) 409–415, http://dx.doi.org/10.1038/nsmb.3194.
[6] T. Theint, P.S. Nadaud, D. Aucoin, J.J. Helmus, S.P. Pondaven, K. Surewicz, et al., Species-dependent structural polymorphism of Y145Stop prion protein amyloid revealed by solid-state NMR spectroscopy, Nat. Commun. 8 (2017) 753, http://dx.doi.org/10.1038/s41467-017-00794-z.
[7] H.-K. Lin, J.C. Boatz, I.E. Krabbendam, R. Kodali, Z. Hou, R. Wetzel, et al., Fibril polymorphism affects immobilized non-amyloid flanking domains of huntingtin exon1 rather than its polyglutamine core, Nat. Commun. 8 (2017) 15462, http://dx.doi.org/10.1038/ncomms15462.
[8] J.C. Boatz, M.J. Whitley, M. Li, A.M. Gronenborn, P.C.A. van der Wel, Cataract-associated P23T γD-crystallin retains a native-like fold in amorphous-looking aggregates formed at physiological pH, Nat. Commun. 8 (2017) 15137, http://dx.doi.org/10.1038/ncomms15137.
[9] D.T. Murray, M. Kato, Y. Lin, K.R. Thurber, I. Hung, S.L. McKnight, et al., Structure of FUS protein fibrils and its relevance to self-assembly and phase separation of low-complexity domains, Cell 171 (2017) 615–627, http://dx.doi.org/10.1016/j.cell.2017.08.048.
[10] M.R. Elkins, T. Wang, M. Nick, H. Jo, T. Lemmin, S.B. Prusiner, et al., Structural polymorphism of Alzheimer's β-amyloid fibrils as controlled by an E22 switch: a solid-state NMR study, J. Am. Chem. Soc. 138 (2016) 9840–9852, http://dx.doi.org/10.1021/jacs.6b03715.
[11] J. Li, T. McQuade, A.B. Siemer, J. Napetschnig, K. Moriwaki, Y.-S. Hsiao, et al., The RIP1/RIP3 necrosome forms a functional amyloid signaling complex required for programmed necrosis, Cell 150 (2012) 339–350, http://dx.doi.org/10.1016/j.cell.2012.06.019.
[12] J.M. Lamley, D. Iuga, C. Öster, H.-J. Sass, M. Rogowski, A. Oss, et al., Solid-state NMR of a protein in a precipitated complex with a full-length antibody, J. Am. Chem. Soc. 136 (2014) 16800–16806, http://dx.doi.org/10.1021/ja5069992.
[13] C. Guo, C. Guo, G. Hou, X. Lu, T. Polenova, Mapping protein–protein interactions by double-REDOR-filtered magic angle spinning NMR spectroscopy, J. Biomol. NMR 67 (2017) 95–108, http://dx.doi.org/10.1007/s10858-016-0086-1.
[14] J. Hu, R. Fu, K. Nishimura, L. Zhang, H.-X. Zhou, D.D. Busath, et al., Histidines, heart of the hydrogen ion channel from influenza A virus: toward an understanding of conductance and proton selectivity, Proc. Natl. Acad. Sci. U.S.A. 103 (2006) 6865–6870, http://dx.doi.org/10.1073/pnas.0601944103.
[15] K.K. Kumashiro, K. Schmidt-Rohr, O.J. Murphy, K. Ouellette, W. Cramer, L.K. Thompson, A novel tool for probing membrane protein structure: Solid-state NMR with proton spin diffusion and X-nucleus detection, J. Am. Chem. Soc. 120 (1998) 5043–5051, http://dx.doi.org/10.1021/ja972655e.
[16] R. Mani, S.D. Cady, M. Tang, A.J. Waring, R.I. Lehrer, M. Hong, Membrane-dependent oligomeric structure and pore formation of a beta-hairpin antimicrobial peptide in lipid bilayers from solid-state NMR, Proc. Natl. Acad. Sci. U.S.A. 103 (2006) 16242–16247, http://dx.doi.org/10.1073/pnas.0605079103.
[17] C. Ader, R. Schneider, S. Hornig, P. Velisetty, E.M. Wilson, A. Lange, et al., A structural link between inactivation and block of a K+ channel, Nat. Struct. Mol. Biol. 15 (2008) 605–612, http://dx.doi.org/10.1038/nsmb.1430.
[18] M.P. Bhate, B.J. Wylie, L. Tian, A.E. McDermott, Conformational dynamics in the selectivity filter of KcsA in response to potassium ion concentration, J. Mol. Biol. 401 (2010) 155–166, http://dx.doi.org/10.1016/j.jmb.2010.06.031.
[19] S.H. Park, B.B. Das, F. Casagrande, Y. Tian, H.J. Nothnagel, M. Chu, et al., Structure of the chemokine receptor CXCR1 in phospholipid bilayers, Nature 253 (2012) 1278, http://dx.doi.org/10.1038/nature11580.
[20] M. Tang, A.E. Nesbitt, L.J. Sperling, D.A. Berthold, C.D. Schwieters, R.B. Gennis, et al., Structure of the disulfide bond generating membrane protein DsbB in the lipid bilayer, J. Mol. Biol. 425 (2013) 1670–1682, http://dx.doi.org/10.1016/j.jmb.2013.02.009.
[21] M. Gustavsson, R. Verardi, D.G. Mullen, K.R. Mote, N.J. Traaseth, T. Gopinath, et al., Allosteric regulation of SERCA by phosphorylation-mediated conformational shift of phospholamban, Proc. Natl. Acad. Sci. U.S.A. 110 (2013) 17338–17343, http://dx.doi.org/10.1073/pnas.1303006110.
[22] A. Mandal, C.L. Hoop, M. DeLucia, R. Kodali, V.E. Kagan, J. Ahn, et al., Structural changes and proapoptotic peroxidase activity of cardiolipin-bound mitochondrial cytochrome *c*, Biophys. J . 109 (2015) 1873–1884, http://dx.doi.org/10.1016/j.bpj.2015.09.016.
[23] M. Kashefi, L.K. Thompson, Signaling-related mobility changes in bacterial chemotaxis receptors revealed by solid-state NMR, J. Phys. Chem. B 121 (2017) 8693–8705, http://dx.doi.org/10.1021/acs.jpcb.7b06475.
[24] D. Good, C. Pham, J. Jagas, J.R. Lewandowski, V. Ladizhansky, Solid-state NMR provides evidence for small-amplitude slow domain motions in a multispanning transmembrane α-helical protein, J. Am. Chem. Soc. 139 (2017) 9246–9258, http://dx.doi.org/10.1021/jacs.7b03974.
[25] M. Yi, T.A. Cross, H.-X. Zhou, Conformational heterogeneity of the M2 proton channel and a structural model for channel activation, Proc. Natl. Acad. Sci. U.S.A. 106 (2009) 13311–13316, http://dx.doi.org/10.1073/pnas.0906553106.
[26] S.D. Cady, K. Schmidt-Rohr, J. Wang, C.S. Soto, W.F. DeGrado, M. Hong, Structure of the amantadine binding site of influenza M2 proton channels in lipid bilayers, Nature 463 (2010) 689–692, http://dx.doi.org/10.1038/nature08722.
[27] F. Hu, W. Luo, M. Hong, Mechanisms of proton conduction and gating in influenza M2 proton channels from solid-state NMR, Science (New York, NY) 330 (2010) 505–508, http://dx.doi.org/10.1126/science.1191714.
[28] J.L. Lorieau, L.A. Day, A.E. McDermott, Conformational dynamics of an intact virus: order parameters for the coat protein of Pf1 bacteriophage, Proc. Natl. Acad. Sci. U.S.A. 105 (2008) 10366–10371, http://dx.doi.org/10.1073/pnas.0800405105.
[29] S.H. Park, F.M. Marassi, D. Black, S.J. Opella, Structure and dynamics of the membrane-bound form of Pf1 coat protein: implications of structural rearrangement for virus assembly, Biophys. J . 99 (2010) 1465–1474, http://dx.doi.org/10.1016/j.bpj.2010.06.009.
[30] M. Wang, C.M. Quinn, J.R. Perilla, H. Zhang, R. Shirra, R. Shirra Jret al., Quenching protein dynamics interferes with HIV capsid maturation, Nat. Commun. 8 (2017) 484–512, http://dx.doi.org/10.1038/s41467-017-01856-y.
[31] C. Liu, C. Liu, J.R. Perilla, J. Ning, M. Lu, G. Hou, et al., Cyclophilin A stabilizes the HIV-1 capsid through a novel non-canonical binding site, 10714 10, Nat. Commun. 7 (2016), http://dx.doi.org/10.1038/ncomms10714.
[32] G. Abramov, R. Shaharabani, O. Morag, R. Avinery, A. Haimovich, I. Oz, et al., Structural effects of single mutations in a filamentous viral capsid across multiple length scales, Biomacromolecules 18 (2017) 2258–2266, http://dx.doi.org/10.1021/acs.biomac.7b00125.
[33] O. Morag, N.G. Sgourakis, D. Baker, A. Goldbourt, The NMR-Rosetta capsid model of M13 bacteriophage reveals a quadrupled hydrophobic packing epitope, Proc. Natl. Acad. Sci. U.S.A. 112 (2015) 971–976, http://dx.doi.org/10.1073/pnas.1415393112.
[34] S. Reckel, J.J. Lopez, F. Löhr, C. Glaubitz, V. Dötsch, In-cell solid-state NMR as a tool to study proteins in large complexes, ChemBioChem 13 (2012) 534–537, http://dx.doi.org/10.1002/cbic.201100721.
[35] X.L. Warnet, A.A. Arnold, I. Marcotte, D.E. Warschawski, In-cell solid-state NMR: An emerging technique for the study of biological membranes, Biophys. J . 109 (2015) 2461–2466, http://dx.doi.org/10.1016/j.bpj.2015.10.041.
[36] M. Renault, R. Tommassen-van Boxtel, M.P. Bos, J.A. Post, J. Tommassen, M. Baldus, Cellular solid-state nuclear magnetic resonance spectroscopy, Proc. Natl. Acad. Sci. U.S.A. 109 (2012) 4863–4868, http://dx.doi.org/10.1073/pnas.1116478109.
[37] D. Huster, J.R. Schiller, K. Arnold, Comparison of collagen dynamics in articular cartilage and isolated fibrils by solid-state NMR spectroscopy, Magn. Reson. Med. 48 (2002) 624–632, http://dx.doi.org/10.1002/mrm.10272.
[38] O.A. McCrate, X. Zhou, C. Reichhardt, L. Cegelski, Sum of the parts: composition and architecture of the bacterial extracellular matrix, J. Mol. Biol. 425 (2013) 4286–4294, http://dx.doi.org/10.1016/j.jmb.2013.06.022.
[39] W.Y. Chow, R. Rajan, K.H. Muller, D.G. Reid, J.N. Skepper, W.C. Wong, et al., NMR spectroscopy of native and in vitro tissues implicates polyADP ribose in biomineralization, Science (New York, NY) 344 (2014) 742–746, http://dx.doi.org/10.1126/science.1248167.
[40] D.T. Murray, N. Das, T.A. Cross, Solid state NMR strategy for characterizing native membrane protein structures, Acc. Chem. Res. 46 (2013) 2172–2181, http://dx.doi.org/10.1021/ar3003442.
[41] M. Weingarth, M. Baldus, Solid-state NMR-based approaches for supramolecular structure elucidation, Acc. Chem. Res. 46 (2013) 2037–2046, http://dx.doi.org/10.1021/ar300316e.
[42] L.A. Baker, G.E. Folkers, T. Sinnige, K. Houben, M. Kaplan, E.A.W. van der Cruijsen, et al., Magic-angle-spinning solid-state NMR of membrane proteins, Methods Enzymol. 557 (2015) 307–328, http://dx.doi.org/10.1016/bs.mie.2014.12.023.
[43] T. Polenova, R. Gupta, A. Goldbourt, Magic angle spinning NMR spectroscopy: a versatile technique for structural and dynamic analysis of solid-phase systems, Anal. Chem. 87 (2015) 5458–5469, http://dx.doi.org/10.1021/ac504288u.
[44] B.J. Wylie, H.Q. Do, C.G. Borcik, E.P. Hardy, Advances in solid-state NMR of membrane proteins, Mol. Phys. 114 (2016) 3598–3609, http://dx.doi.org/10.1080/00268976.2016.1252470.
[45] C.M. Quinn, T. Polenova, Structural biology of supramolecular assemblies by magic-angle spinning NMR spectroscopy, Q. Rev. Biophys. 50 (2017) e1, http://dx.doi.org/10.1017/S0033583516000159.
[46] S.J. Opella, F.M. Marassi, Applications of NMR to membrane proteins, Arch. Biochem. Biophys. (2017), http://dx.doi.org/10.1016/j.abb.2017.05.011.
[47] B.H. Meier, R. Riek, A. Böckmann, Emerging structural understanding of amyloid fibrils by solid-state NMR, Trends Biochem. Sci. 42 (2017) 777–787, http://dx.doi.org/10.1016/j.tibs.2017.08.001.
[48] R. Linser, Solid-state NMR spectroscopic trends for supramolecular assemblies and protein aggregates, Solid State Nucl. Magn. Reson. 87 (2017) 45–53, http://dx.doi.org/10.1016/j.ssnmr.2017.08.003.
[49] P.C.A. van der Wel, Insights into protein misfolding and aggregation enabled by solid-state NMR spectroscopy, Solid State Nucl. Magn. Reson. 88 (2017) 1–14, http://dx.doi.org/10.1016/j.ssnmr.2017.10.001.
[50] P.C.A. van der Wel, New applications of solid-state NMR in structural biology, Emerg. Top. Life Sci. 2 (2018) 57–67, http://dx.doi.org/10.1042/ETLS20170088.
[51] V.S. Bajaj, P.C.A. van der Wel, R.G. Griffin, Observation of a low-temperature, dynamically driven structural transition in a polypeptide by solid-state NMR spectroscopy, J. Am. Chem. Soc. 131 (2009) 118–128, http://dx.doi.org/10.1021/ja8045926.
[52] J.R. Lewandowski, M.E. Halse, M. Blackledge, L. Emsley, Direct observation of

hierarchical protein dynamics, Science (New York, NY) 348 (2015) 578–581, http://dx.doi.org/10.1126/science.aaa6111.
[53] J.R. Lewandowski, Advances in solid-state relaxation methodology for probing site-specific protein dynamics, Acc. Chem. Res. 46 (2013) 2018–2027, http://dx.doi.org/10.1021/ar300334g.
[54] S.K. Hansen, K. Bertelsen, B. Paaske, N.C. Nielsen, T. Vosegaard, Solid-state NMR methods for oriented membrane proteins, Progr. Nucl. Magn. Reson. Spectrosc. 88–89 (2015) 48–85, http://dx.doi.org/10.1016/j.pnmrs.2015.05.001.
[55] B. Bechinger, E.S. Salnikov, The membrane interactions of antimicrobial peptides revealed by solid-state NMR spectroscopy, Chem. Phys. Lipids 165 (2012) 282–301, http://dx.doi.org/10.1016/j.chemphyslip.2012.01.009.
[56] K. Koch, S. Afonin, M. Ieronimo, M. Berditsch, A.S. Ulrich, Solid-state (19)F-NMR of peptides in native membranes, Top. Curr. Chem. 306 (2011) 89–118, http://dx.doi.org/10.1007/128_2011_162.
[57] M. Hong, Y. Zhang, F. Hu, Membrane protein structure and dynamics from NMR spectroscopy, Annu. Rev. Phys. Chem. 63 (2012) 1–24, http://dx.doi.org/10.1146/annurev-physchem-032511-143731.
[58] S. Yan, C.L. Suiter, G. Hou, H. Zhang, T. Polenova, Probing structure and dynamics of protein assemblies by magic angle spinning NMR spectroscopy, Acc. Chem. Res. 46 (2013) 2047–2058, http://dx.doi.org/10.1021/ar300309s.
[59] A. Krushelnitsky, D. Reichert, K. Saalwächter, Solid-state NMR approaches to internal dynamics of proteins: from picoseconds to microseconds and seconds, Acc. Chem. Res. 46 (2013) 2028–2036, http://dx.doi.org/10.1021/ar300292p.
[60] R. Linser, R. Sarkar, A. Krushelnitzky, A. Mainz, B. Reif, Dynamics in the solid-state: perspectives for the investigation of amyloid aggregates, membrane proteins and soluble protein complexes, J. Biomol. NMR 59 (2014) 1–14, http://dx.doi.org/10.1007/s10858-014-9822-6.
[61] J.M. Lamley, J.R. Lewandowski, Relaxation-based magic-angle spinning NMR approaches for studying protein dynamics, eMagRes. 5 (2016) 1423–1434, http://dx.doi.org/10.1002/9780470034590.emrstm1417.
[62] P. Schanda, M. Ernst, Studying dynamics by magic-angle spinning solid-state NMR spectroscopy: principles and applications to biomolecules, Progr. Nucl. Magn. Reson. Spectrosc. 96 (2016) 1–46, http://dx.doi.org/10.1016/j.pnmrs.2016.02.001.
[63] M. Veshtort, R.G. Griffin, SPINEVOLUTION: a powerful tool for the simulation of solid and liquid state NMR experiments, J. Magn. Reson. 178 (2006) 248–282, http://dx.doi.org/10.1016/j.jmr.2005.07.018.
[64] S. Hartmann, E. Hahn, Nuclear double resonance in the rotating frame, Phys. Rev. 128 (1962) 2042–2053, http://dx.doi.org/10.1103/PhysRev. 128.2042.
[65] A. Pines, M.G. Gibby, J.S. Waugh, Proton-enhanced NMR of dilute spins in solids, J. Chem. Phys. 59 (1973) 569.
[66] G.A. Morris, R. Freeman, Enhancement of nuclear magnetic resonance signals by polarization transfer, J. Am. Chem. Soc. 101 (1979) 760–762, http://dx.doi.org/10.1021/ja00497a058.
[67] G. Hou, S. Ding, L. Zhang, F. Deng, Breaking the T1 constraint for quantitative measurement in magic angle spinning solid-state NMR spectroscopy, J. Am. Chem. Soc. 132 (2010) 5538–5539, http://dx.doi.org/10.1021/ja909550f.
[68] R.L. Johnson, K. Schmidt-Rohr, Quantitative solid-state ^{13}C NMR with signal enhancement by multiple cross polarization, J. Magn. Reson. 239 (2014) 44–49, http://dx.doi.org/10.1016/j.jmr.2013.11.009.
[69] D.A. Torchia, A. Szabo, Spin-lattice relaxation in solids, J. Magn. Reson. 49 (1982) (1969) 107–121, http://dx.doi.org/10.1016/0022-2364(82)90301-8.
[70] J.L. Lorieau, A.E. McDermott, Conformational flexibility of a microcrystalline globular protein: order parameters by solid-state NMR spectroscopy, J. Am. Chem. Soc. 128 (2006) 11505–11512, http://dx.doi.org/10.1021/ja062443u.
[71] V. Chevelkov, U. Fink, B. Reif, Accurate determination of order parameters from ^{1}H,^{15}N dipolar couplings in MAS solid-state NMR experiments, J. Am. Chem. Soc. 131 (2009) 14018–14022, http://dx.doi.org/10.1021/ja902649u.
[72] H.A. Scheidt, I. Morgado, S. Rothemund, D. Huster, Dynamics of amyloid β fibrils revealed by solid-state NMR, J. Biol. Chem. 287 (2012) 2017–2021, http://dx.doi.org/10.1074/jbc.M111.308619.
[73] G. Hou, S. Paramasivam, S. Yan, T. Polenova, A.J. Vega, Multidimensional magic angle spinning NMR spectroscopy for site-resolved measurement of proton chemical shift anisotropy in biological solids, J. Am. Chem. Soc. 135 (2013) 1358–1368, http://dx.doi.org/10.1021/ja3084972.
[74] L. Vugmeyster, M.A. Clark, I.B. Falconer, D. Ostrovsky, D. Gantz, W. Qiang, et al., Flexibility and solvation of amyloid-β hydrophobic core, J. Biol. Chem. 291 (2016) 18484–18495, http://dx.doi.org/10.1074/jbc.M116.740530.
[75] X. Shi, C.M. Rienstra, Site-specific internal motions in GB1 protein microcrystals revealed by 3D ^{2}H–^{13}C–^{13}C solid-state NMR spectroscopy, J. Am. Chem. Soc. 138 (2016) 4105–4119, http://dx.doi.org/10.1021/jacs.5b12974.
[76] X.L. Warnet, M. Laadhari, A.A. Arnold, I. Marcotte, D.E. Warschawski, A 2H magic-angle spinning solid-state NMR characterisation of lipid membranes in intact bacteria, Biochim. Biophys. Acta 2016 (1858) 146–152, http://dx.doi.org/10.1016/j.bbamem.2015.10.020.
[77] J. Yang, M.L. Tasayco, T. Polenova, Dynamics of reassembled thioredoxin studied by magic angle spinning NMR: snapshots from different time scales, J. Am. Chem. Soc. 131 (2009) 13690–13702, http://dx.doi.org/10.1021/ja9037802.
[78] M. Munowitz, R.G. Griffin, G. Bodenhausen, T.H. Huang, Two-dimensional rotational spin-echo nuclear magnetic resonance in solids: correlation of chemical shift and dipolar interactions, J. Am. Chem. Soc. 103 (1981) 2529–2533, http://dx.doi.org/10.1021/ja00400a007.
[79] J.S. Waugh, Uncoupling of local field spectra in nuclear magnetic-resonance – determination of atomic positions in solids, Proc. Natl. Acad. Sci. U.S.A. 73 (1976) 1394–1397.
[80] J.L. Lorieau, A.E. McDermott, Order parameters based on (13)C(1)H, (13)C(1)H (2) and (13)C(1)H(3) heteronuclear dipolar powder patterns: a comparison of MAS-based solid-state NMR sequences, Magn. Reson. Chem. 44 (2006) 334–347, http://dx.doi.org/10.1002/mrc.1773.
[81] G. Hou, I.-J.L. Byeon, J. Ahn, A.M. Gronenborn, T. Polenova, ^{1}H-^{13}C/^{1}H-^{15}N heteronuclear dipolar recoupling by R-symmetry sequences under fast magic angle spinning for dynamics analysis of biological and organic solids, J. Am. Chem. Soc. 133 (2011) 18646–18655, http://dx.doi.org/10.1021/ja203771a.
[82] R.H. Newman, L.M. Condron, Separating subspectra from cross-polarization magic-angle spinning nuclear magnetic resonance spectra by proton spin relaxation editing, Solid State Nucl. Magn. Reson. 4 (1995) 259–266, http://dx.doi.org/10.1016/0926-2040(94)00047-G.
[83] D. Huster, S. Yamaguchi, M. Hong, Efficient beta-sheet identification in proteins by solid-state NMR spectroscopy, J. Am. Chem. Soc. 122 (2000) 11320–11327, http://dx.doi.org/10.1021/ja001674c.
[84] H.-R. Tang, Y.-L. Wang, P.S. Belton, ^{13}C CPMAS studies of plant cell wall materials and model systems using proton relaxation-induced spectral editing techniques, Solid State Nucl. Magn. Reson. 15 (2000) 239–248, http://dx.doi.org/10.1016/S0926-2040(99)00064-8.
[85] D. Sakellariou, A. Lesage, L. Emsley, Spectral editing in solid-state NMR using scalar multiple quantum filters, J. Magn. Reson. 151 (2001) 40–47, http://dx.doi.org/10.1006/jmre.2001.2338.
[86] D. Huster, X. Yao, M. Hong, Membrane protein topology probed by (1)H spin diffusion from lipids using solid-state NMR spectroscopy, J. Am. Chem. Soc. 124 (2002) 874–883, http://dx.doi.org/10.1021/ja017001r.
[87] H. Tang, B.P. Hills, Use of (13)C MAS NMR to study domain structure and dynamics of polysaccharides in the native starch granules, Biomacromolecules 4 (2003) 1269–1276, http://dx.doi.org/10.1021/bm0340772.
[88] S. Jehle, M. Hiller, K. Rehbein, A. Diehl, H. Oschkinat, B.-J. van Rossum, Spectral editing: selection of methyl groups in multidimensional solid-state magic-angle spinning NMR, J. Biomol. NMR 36 (2006) 169–177, http://dx.doi.org/10.1007/s10858-006-9078-x.
[89] K. Schmidt-Rohr, K.J. Fritzsching, S.Y. Liao, M. Hong, Spectral editing of two-dimensional magic-angle-spinning solid-state NMR spectra for protein resonance assignment and structure determination, J. Biomol. NMR 54 (2012) 343–353, http://dx.doi.org/10.1007/s10858-012-9676-8.
[90] D. Huster, P.K. Madhu, Simplifying solid-state NMR spectra for biophysical studies on membrane proteins: selective targeting of sites and interactions, Biophys. J. 106 (2014) 2083–2084, http://dx.doi.org/10.1016/j.bpj.2014.04.019.
[91] M.H. Frey, J. DiVerdi, S.J. Opella, Dynamics of phenylalanine in the solid state by NMR, J. Am. Chem. Soc. 107 (1985) 7311–7315.
[92] H. Heise, W. Hoyer, S. Becker, O.C. Andronesi, D. Riedel, M. Baldus, Molecular-level secondary structure, polymorphism, and dynamics of full-length alpha-synuclein fibrils studied by solid-state NMR, Proc. Natl. Acad. Sci. U.S.A. 102 (2005) 15871–15876, http://dx.doi.org/10.1073/pnas.0506109102.
[93] J. Yang, L. Aslimovska, C. Glaubitz, Molecular dynamics of proteorhodopsin in lipid bilayers by solid-state NMR, J. Am. Chem. Soc. 133 (2011) 4874–4881, http://dx.doi.org/10.1021/ja109766n.
[94] D.B. Good, S. Wang, M.E. Ward, J. Struppe, L.S. Brown, J.R. Lewandowski, et al., Conformational dynamics of a seven transmembrane helical protein Anabaena Sensory Rhodopsin probed by solid-state NMR, J. Am. Chem. Soc. 136 (2014) 2833–2842, http://dx.doi.org/10.1021/ja411633w.
[95] V. Chevelkov, A.V. Zhuravleva, Y. Xue, B. Reif, N.R. Skrynnikov, Combined analysis of (15)N relaxation data from solid- and solution-state NMR spectroscopy, J. Am. Chem. Soc. 129 (2007) 12594–12595, http://dx.doi.org/10.1021/ja073234s.
[96] E.A. Fry, S. Sengupta, V.C. Phan, S. Kuang, K.W. Zilm, CSA-enabled spin diffusion leads to MAS rate-dependent T1's at high field, J. Am. Chem. Soc. 133 (2011) 1156–1158, http://dx.doi.org/10.1021/ja106730p.
[97] A. Kalk, H.J.C. Berendsen, Proton magnetic relaxation and spin diffusion in proteins, J. Magn. Reson. 24 (1976) (1969) 343–366, http://dx.doi.org/10.1016/0022-2364(76)90115-3.
[98] R.A. Olsen, J. Struppe, D.W. Elliott, R.J. Thomas, L.J. Mueller, Through-bond ^{13}C–^{13}C correlation at the natural abundance level: refining dynamic regions in the crystal structure of vitamin-D_3 with solid-state NMR, J. Am. Chem. Soc. 125 (2003) 11784–11785, http://dx.doi.org/10.1021/ja036655s.
[99] O.C. Andronesi, S. Becker, K. Seidel, H. Heise, H.S. Young, M. Baldus, Determination of membrane protein structure and dynamics by magic-angle-spinning solid-state NMR spectroscopy, J. Am. Chem. Soc. 127 (2005) 12965–12974, http://dx.doi.org/10.1021/ja0530164.
[100] A.B. Siemer, A.A. Arnold, C. Ritter, T. Westfeld, M. Ernst, R. Riek, et al., Observation of highly flexible residues in amyloid fibrils of the HET-s prion, J. Am. Chem. Soc. 128 (2006) 13224–13228, http://dx.doi.org/10.1021/ja063639x.
[101] A.S. Falk, A.B. Siemer, Dynamic domains of amyloid fibrils can be site-specifically assigned with proton detected 3D NMR spectroscopy, J. Biomol. NMR 66 (2016) 159–162, http://dx.doi.org/10.1007/s10858-016-0069-2.
[102] L. Zhong, L. Zhong, V.V. Bamm, M.A.M. Ahmed, G. Harauz, V. Ladizhansky, Solid-state NMR spectroscopy of 18.5 kDa myelin basic protein reconstituted with lipid vesicles: spectroscopic characterisation and spectral assignments of solvent-exposed protein fragments, Biochim. Biophys. Acta 1768 (2007) 3193–3205, http://dx.doi.org/10.1016/j.bbamem.2007.08.013.
[103] M. Baldus, B.H. Meier, Total correlation spectroscopy in the solid state. The use of scalar couplings to determine the through-bond connectivity, J. Magn. Reson., Ser. A 121 (1996) 65–69.
[104] L. Chen, R.A. Olsen, D.W. Elliott, J.M. Boettcher, D.H. Zhou, C.M. Rienstra, et al., Constant-time through-bond ^{13}C correlation spectroscopy for assigning protein resonances with solid-state NMR spectroscopy, J. Am. Chem. Soc. 128 (2006) 9992–9993, http://dx.doi.org/10.1021/ja062347t.

[105] E. Barbet-Massin, A.J. Pell, M.J. Knight, A.L. Webber, I.C. Felli, R. Pierattelli, et al., ^{13}C-detected through-bond correlation experiments for protein resonance assignment by ultra-fast MAS solid-state NMR, ChemPhysChem 14 (2013) 3131–3137, http://dx.doi.org/10.1002/cphc.201201097.
[106] G.S. Harbison, J. Roberts, J. Herzfeld, R.G. Griffin, Solid-state NMR detection of proton exchange between the bacteriorhodopsin Schiff base and bulk water, J. Am. Chem. Soc. 110 (1988) 7221–7223.
[107] C. Ader, R. Schneider, K. Seidel, M. Etzkorn, S. Becker, M. Baldus, Structural rearrangements of membrane proteins probed by water-edited solid-state NMR spectroscopy, J. Am. Chem. Soc. 131 (2009) 170–176, http://dx.doi.org/10.1021/ja806306e.
[108] J. Yang, M.L. Tasayco, T. Polenova, Magic angle spinning NMR experiments for structural studies of differentially enriched protein interfaces and protein assemblies, J. Am. Chem. Soc. 130 (2008) 5798–5807, http://dx.doi.org/10.1021/ja711304e.
[109] M.A. Caporini, C.J. Turner, A. Bielecki, R.G. Griffin, Chemical shift anisotropy selective inversion, J. Magn. Reson. 200 (2009) 233–238, http://dx.doi.org/10.1016/j.jmr.2009.07.003.
[110] A.D. Merg, J.C. Boatz, A. Mandal, G. Zhao, S. Mokashi-Punekar, C. Liu, et al., Peptide-directed assembly of single-helical gold nanoparticle superstructures exhibiting intense chiroptical activity, J. Am. Chem. Soc. 138 (2016) 13655–13663, http://dx.doi.org/10.1021/jacs.6b07322.
[111] A. Witkowski, G.K.L. Chan, J.C. Boatz, N.J. Li, A.P. Inoue, J.C. Wong, et al., Methionine oxidized apolipoprotein A-I at the crossroads of HDL biogenesis and amyloid formation, FASEB J. (2018), http://dx.doi.org/10.1096/fj.201701127Rfj.201701127R, (in press).
[112] R. Tycko, Physical and structural basis for polymorphism in amyloid fibrils, Protein Sci. 23 (2014) 1528–1539, http://dx.doi.org/10.1002/pro.2544.
[113] G. Comellas, C.M. Rienstra, Protein structure determination by magic-angle spinning solid-state NMR, and insights into the formation, structure, and stability of amyloid fibrils, Annu. Rev. Biophys. 42 (2013) 515–536, http://dx.doi.org/10.1146/annurev-biophys-083012-130356.
[114] R. Schneider, M.C. Schumacher, H. Mueller, D. Nand, V. Klaukien, H. Heise, et al., Structural characterization of polyglutamine fibrils by solid-state NMR spectroscopy, J. Mol. Biol. 412 (2011) 121–136, http://dx.doi.org/10.1016/j.jmb.2011.06.045.
[115] V.N. Sivanandam, M. Jayaraman, C.L. Hoop, R. Kodali, R. Wetzel, P.C.A. van der Wel, The aggregation-enhancing huntingtin N-terminus is helical in amyloid fibrils, J. Am. Chem. Soc. 133 (2011) 4558–4566, http://dx.doi.org/10.1021/ja110715f.
[116] K. Kar, C.L. Hoop, K.W. Drombosky, M.A. Baker, R. Kodali, I. Arduini, et al., β-hairpin-mediated nucleation of polyglutamine amyloid formation, J. Mol. Biol. 425 (2013) 1183–1197, http://dx.doi.org/10.1016/j.jmb.2013.01.016.
[117] C.L. Hoop, H.-K. Lin, K. Kar, Z. Hou, M.A. Poirier, R. Wetzel, et al., Polyglutamine amyloid core boundaries and flanking domain dynamics in huntingtin fragment fibrils determined by solid-state nuclear magnetic resonance, Biochemistry 53 (2014) 6653–6666, http://dx.doi.org/10.1021/bi501010q.
[118] J.M. Isas, R. Langen, A.B. Siemer, Solid-state nuclear magnetic resonance on the static and dynamic domains of huntingtin exon-1 fibrils, Biochemistry 54 (2015) 3942–3949, http://dx.doi.org/10.1021/acs.biochem.5b00281.
[119] C.L. Hoop, H.-K. Lin, K. Kar, G. Magyarfalvi, J.M. Lamley, J.C. Boatz, et al., Huntingtin exon 1 fibrils feature an interdigitated β-hairpin-based polyglutamine core, Proc. Natl. Acad. Sci. U.S.A. 113 (2016) 1546–1551, http://dx.doi.org/10.1073/pnas.1521933113.
[120] J.M. Isas, A. Langen, M.C. Isas, N.K. Pandey, A.B. Siemer, Formation and structure of wild type huntingtin exon-1 fibrils, Biochemistry 56 (2017) 3579–3586, http://dx.doi.org/10.1021/acs.biochem.7b00138.
[121] The Huntingon's Disease Collaborative Group, A novel gene containing a trinucleotide repeat that is expanded and unstable on Huntington's disease chromosomes, Cell 72 (1993) 971–983, http://dx.doi.org/10.1016/0092-8674(93)90585-E.
[122] A. Böckmann, C. Gardiennet, R. Verel, A. Hunkeler, A. Loquet, G. Pintacuda, et al., Characterization of different water pools in solid-state NMR protein samples, J. Biomol. NMR 45 (2009) 319–327, http://dx.doi.org/10.1007/s10858-009-9374-3.
[123] A. Mandal, J.C. Boatz, T.B. Wheeler, P.C.A. van der Wel, On the use of ultracentrifugal devices for routine sample preparation in biomolecular magic-angle-spinning NMR, J. Biomol. NMR 67 (2017) 165–178, http://dx.doi.org/10.1007/s10858-017-0089-6.
[124] K. Takegoshi, S. Nakamura, T. Terao, ^{13}C-^{1}H dipolar-assisted rotational resonance in magic-angle spinning NMR, Chem. Phys. Lett. 344 (2001) 631–637, http://dx.doi.org/10.1016/S0009-2614(01)00791-6.
[125] K.J. Fritzsching, Y. Yang, K. Schmidt-Rohr, M. Hong, Practical use of chemical shift databases for protein solid-state NMR: 2D chemical shift maps and amino-acid assignment with secondary-structure information, J. Biomol. NMR 56 (2013) 155–167, http://dx.doi.org/10.1007/s10858-013-9732-z.
[126] J.R. Lewandowski, J. Sein, H.J. Sass, S. Grzesiek, M. Blackledge, L. Emsley, Measurement of site-specific ^{13}C spin–lattice relaxation in a crystalline protein, J. Am. Chem. Soc. 132 (2010) 8252–8254, http://dx.doi.org/10.1021/ja102744b.
[127] J.D. Haller, P. Schanda, Amplitudes and time scales of picosecond-to-microsecond motion in proteins studied by solid-state NMR: a critical evaluation of experimental approaches and application to crystalline ubiquitin, J. Biomol. NMR 57 (2013) 263–280, http://dx.doi.org/10.1007/s10858-013-9787-x.
[128] F.J.B. Bäuerlein, I. Saha, A. Mishra, M. Kalemanov, A. Martínez-Sánchez, R. Klein, et al., In situ architecture and cellular interactions of PolyQ inclusions, Cell 171 (2017) 179–187, http://dx.doi.org/10.1016/j.cell.2017.08.009.
[129] S.H. Shahmoradian, J.G. Galaz-Montoya, M.F. Schmid, Y. Cong, B. Ma, C. Spiess, et al., TRiC's tricks inhibit Huntingtin aggregation, eLife 2 (2013) e00710, http://dx.doi.org/10.7554/eLife.00710.
[130] Q. Guo, Bin Huang, J. Cheng, M. Seefelder, T. Engler, G. Pfeifer, et al., The cryo-electron microscopy structure of huntingtin, Nature 555 (2018) 117–120, http://dx.doi.org/10.1038/nature25502.
[131] A.W.P. Fitzpatrick, B. Falcon, S. He, A.G. Murzin, G. Murshudov, H.J. Garringer, et al., Cryo-EM structures of tau filaments from Alzheimer's disease, Nature 56 (2017) 343, http://dx.doi.org/10.1038/nature23002.
[132] J.J. Helmus, K. Surewicz, W.K. Surewicz, C.P. Jaroniec, Conformational flexibility of Y145Stop human prion protein amyloid fibrils probed by solid-state nuclear magnetic resonance spectroscopy, J. Am. Chem. Soc. 132 (2010) 2393–2403, http://dx.doi.org/10.1021/ja909827v.
[133] P. Schmidt, L. Thomas, P. Müller, H.A. Scheidt, D. Huster, The G-protein-coupled neuropeptide Y receptor type 2 is highly dynamic in lipid membranes as revealed by solid-state NMR spectroscopy, Chemistry 20 (2014) 4986–4992, http://dx.doi.org/10.1002/chem.201304928.
[134] R. Huang, K. Yamamoto, M. Zhang, N. Popovych, I. Hung, S.-C. Im, et al., Probing the transmembrane structure and dynamics of microsomal NADPH-cytochrome P450 oxidoreductase by solid-state NMR, Biophys. J. 106 (2014) 2126–2133, http://dx.doi.org/10.1016/j.bpj.2014.03.051.
[135] M. Gopalswamy, A. Kumar, J. Adler, M. Baumann, M. Henze, S.T. Kumar, et al., Structural characterization of amyloid fibrils from the human parathyroid hormone, Biochim. Biophys. Acta, Proteins Proteomics 2015 (1854) 249–257, http://dx.doi.org/10.1016/j.bbapap.2014.12.020.
[136] M.E. Ward, E. Ritz, M.A.M. Ahmed, V.V. Bamm, G. Harauz, L.S. Brown, et al., Proton detection for signal enhancement in solid-state NMR experiments on mobile species in membrane proteins, J. Biomol. NMR 63 (2015) 375–388, http://dx.doi.org/10.1007/s10858-015-9997-5.
[137] T. Gopinath, S.E.D. Nelson, K.J. Soller, G. Veglia, Probing the conformationally excited states of membrane proteins via ^{1}H-detected MAS solid-state NMR spectroscopy, J. Phys. Chem. B 121 (2017) 4456–4465, http://dx.doi.org/10.1021/acs.jpcb.7b03268.
[138] J.D. Gross, P.R. Costa, J.P. Dubacq, D.E. Warschawski, P.N. Lirsac, P.F. Devaux, et al., Multidimensional NMR in lipid systems. Coherence transfer through J couplings under MAS, J. Magn. Reson. B 106 (1995) 187–190, http://dx.doi.org/10.1006/jmrb.1995.1031.
[139] J. Forbes, C. Husted, E. Oldfield, High-field, high-resolution proton "magic-angle" sample-spinning nuclear magnetic resonance spectroscopic studies of gel and liquid crystalline lipid bilayers and the effects of cholesterol, J. Am. Chem. Soc. 110 (1988) 1059–1065, http://dx.doi.org/10.1021/ja00212a010.
[140] D.E. Warschawski, P.F. Devaux, Polarization transfer in lipid membranes, J. Magn. Reson. 145 (2000) 367–372, http://dx.doi.org/10.1006/jmre.2000.2135.
[141] M. Etzkorn, S. Martell, O.C. Andronesi, K. Seidel, M. Engelhard, M. Baldus, Secondary structure, dynamics, and topology of a seven-helix receptor in native membranes, studied by solid-state NMR spectroscopy, Angew. Chem. Int. Ed. Engl. 46 (2007) 459–462, http://dx.doi.org/10.1002/anie.200602139.
[142] M. Hong, K. Schmidt-Rohr, Magic-angle-spinning NMR techniques for measuring long-range distances in biological macromolecules, Acc. Chem. Res. 46 (2013) 2154–2163, http://dx.doi.org/10.1021/ar300294x.
[143] S.A. Cervantes, T.H. Bajakian, M.A. Soria, A.S. Falk, R.J. Service, R. Langen, et al., Identification and structural characterization of the N-terminal amyloid core of Orb2 isoform A, Sci. Rep. 6 (2016) 38265, http://dx.doi.org/10.1038/srep38265.
[144] B.L. Raveendra, A.B. Siemer, S.V. Puthanveettil, W.A. Hendrickson, E.R. Kandel, A.E. McDermott, Characterization of prion-like conformational changes of the neuronal isoform of aplysia CPEB, Nat. Struct. Mol. Biol. 20 (2013) 495–501, http://dx.doi.org/10.1038/nsmb.2503.
[145] A.B. Siemer, C. Ritter, M.O. Steinmetz, M. Ernst, R. Riek, B.H. Meier, ^{13}C, ^{15}N resonance assignment of parts of the HET-s prion protein in its amyloid form, J. Biomol. NMR 34 (2006) 75–87, http://dx.doi.org/10.1007/s10858-005-5582-7.
[146] J.R. Lewandowski, P.C.A. van der Wel, M. Rigney, N. Grigorieff, R.G. Griffin, Structural complexity of a composite amyloid fibril, J. Am. Chem. Soc. 133 (2011) 14686–14698, http://dx.doi.org/10.1021/ja203736z.
[147] Y.L. Mobarhan, B. Fortier-McGill, R. Soong, W.E. Maas, M. Fey, M. Monette, et al., Comprehensive multiphase NMR applied to a living organism, Chem. Sci. 7 (2016) 4856–4866, http://dx.doi.org/10.1039/C6SC00329J.
[148] H.R. Tang, P.S. Belton, Molecular dynamics of polycrystalline cellobiose studied by solid-state NMR, Solid State Nucl. Magn. Reson. 21 (2002) 117–133, http://dx.doi.org/10.1006/snmr.2002.0052.
[149] D. Courtier-Murias, H. Farooq, H. Masoom, A. Botana, R. Soong, J.G. Longstaffe, et al., Comprehensive multiphase NMR spectroscopy: basic experimental approaches to differentiate phases in heterogeneous samples, J. Magn. Reson. 217 (2012) 61–76, http://dx.doi.org/10.1016/j.jmr.2012.02.009.
[150] T. Iline-Vul, I. Matlahov, J. Grinblat, K. Keinan-Adamsky, G. Goobes, Changes to the disordered phase and apatite crystallite morphology during mineralization by an acidic mineral binding peptide from osteonectin, Biomacromolecules 16 (2015) 2656–2663, http://dx.doi.org/10.1021/acs.biomac.5b00465.
[151] K.H. Mroue, J. Xu, P. Zhu, M.D. Morris, A. Ramamoorthy, Selective detection and complete identification of triglycerides in cortical bone by high-resolution ^{1}H MAS NMR spectroscopy, Phys. Chem. Chem. Phys. 18 (2016) 18687–18691, http://dx.doi.org/10.1039/C6CP03506J.